

คอมพอสิตของอนุภาคแม่เหล็กระดับนาโนเมตรและเมโซพอร์สซิลิกาเอ็มซีเอ็ม-48

สำหรับการจัดไอออนปรอท (II)

นางสาวสมิตรา คนสง่า

วิทยานิพนธ์นี้เป็นส่วนหนึ่งของการศึกษาตามหลักสูตรปริญญาวิทยาศาสตรมหาบัณฑิต

สาขาวิชาปิโตรเคมีและวิทยาศาสตร์พอลิเมอร์

คณะวิทยาศาสตร์ จุฬาลงกรณ์มหาวิทยาลัย

ปีการศึกษา 2555

ลิขสิทธิ์ของจุฬาลงกรณ์มหาวิทยาลัย

บทคัดย่อและแฟ้มข้อมูลฉบับเต็มของวิทยานิพนธ์ตั้งแต่ปีการศึกษา 2554 ที่ให้บริการในคลังปัญญาจุฬาฯ (CUIR)  
เป็นแฟ้มข้อมูลของนิสิตเจ้าของวิทยานิพนธ์ที่ส่งผ่านทางบัณฑิตวิทยาลัย

The abstract and full text of theses from the academic year 2011 in Chulalongkorn University Intellectual Repository (CUIR)  
are the thesis authors' files submitted through the Graduate School.

MAGNETIC NANOPARTICLE-MESOPOROUS SILICA MCM-48 COMPOSITES FOR  
MERCURY(II) ION REMOVAL

Miss Sumitra Khonsa-nga

A Thesis Submitted in Partial Fulfillment of the Requirements  
for the Degree of Master of Science Program in Petrochemistry and Polymer Science

Faculty of Science

Chulalongkorn University

Academic Year 2012

Copyright of Chulalongkorn University

Thesis Title                                   MAGNETIC NANOPARTICLE-MESOPOROUS SILICA  
MCM-48 COMPOSITES FOR MERCURY(II) ION  
REMOVAL

By   Miss Sumitra Khonsa-nga

Field of Study                                 Petrochemistry and Polymer Science

Thesis Advisor                               Assistant Professor Fuangfa Unob, Ph.D.

Thesis Co-advisor                          Numpon Insin, Ph.D.

---

Accepted by the Faculty of Science, Chulalongkorn University in Partial  
Fulfillment of the Requirements for the Master's Degree

.....Dean of the Faculty of Science  
(Professor Supot Hannongbua, Dr.rer.nat.)

#### THESIS COMMITTEE

.....Chairman  
(Assistant Professor Warinthorn Chavasiri, Ph.D.)

.....Thesis Advisor  
(Assistant Professor Fuangfa Unob, Ph.D.)

.....Thesis Co-Advisor  
(Numpon Insin, Ph.D.)

.....Examiner  
(Associate Professor Wimonrat Trakarnpruk, Ph.D.)

.....External Examiner  
(Vuthichai Ervithayasuporn, Ph.D.)

สมิตรา คนสง่า : คอมพอสิตของอนุภาคแม่เหล็กระดับนาโนเมตรและเมโซพอร์ซิลิกาเอ็มซีเอ็ม-48 สำหรับการขจัดไอออนปรอท (II). (MAGNETIC NANOPARTICLE-MESOPOROUS SILICA MCM-48 COMPOSITES FOR MERCURY(II) ION REMOVAL) อ.ที่ปรึกษาวิทยานิพนธ์หลัก : ผศ.ดร.เฟื่องฟ้า อุ่ณอบ, อ.ที่ปรึกษาวิทยานิพนธ์ร่วม : อ.ดร.นำพล อินสิน, 65 หน้า.

ตัวดูดซับMCM-48ชนิดใหม่ซึ่งมีสมบัติแม่เหล็กและมีหมู่ฟังก์ชันไฮดรอกซิล(MP-Fe<sub>2</sub>O<sub>3</sub>@MCM-48) ได้ถูกสังเคราะห์ขึ้นเพื่อการใช้งานในการขจัดปรอท พื้นที่ผิวของMCM-48, γ-Fe<sub>2</sub>O<sub>3</sub>@MCM-48 และ MP-Fe<sub>2</sub>O<sub>3</sub>@MCM-48 คือ 941.67, 850.16 และ 677.58 ตารางเมตรต่อกรัมตามลำดับ ผลิตภัณฑ์ที่ได้ถูกพิสูจน์เอกลักษณ์โดยอาศัยเทคนิค เอ็กซ์เรย์ดิฟแฟรกชัน พูเรียร์ ทรานสฟอร์มอินฟราเรดสเปกโทรสโกปี กล้องจุลทรรศน์อิเล็กตรอนแบบส่องกราด และกล้องจุลทรรศน์อิเล็กตรอนแบบส่องผ่าน จากนั้นศึกษาการดูดซับไอออนปรอทด้วย MP-Fe<sub>2</sub>O<sub>3</sub>@MCM-48 โดยใช้วิธีแบบทซ์ ใช้ปริมาณตัวดูดซับในสัดส่วน 2 กรัมต่อลิตรสารละลาย ทำการศึกษาผลของพีเอชของสารละลายและเวลาที่ใช้ในการสกัด โดยภาวะที่เหมาะสมในการดูดซับไอออนปรอทของ MP-Fe<sub>2</sub>O<sub>3</sub>@MCM-48 คือ ที่พีเอชเท่ากับ 6 และเวลาในการดูดซับ 60 นาที พฤติกรรมการดูดซับไอออนปรอทด้วยตัวดูดซับเป็นไปตามไอโซเทอมของแลงเมียร์ ซึ่งคำนวณค่าความจุการดูดซับสูงสุดได้ 208.3 มิลลิกรัมต่อกรัมตัวดูดซับ สามารถนำตัวดูดซับมาใช้ซ้ำได้ 4 ครั้ง โดยใช้สารละลายไทโอยูเรีย 1.0 โมลต่อลิตรในสารละลายกรดไนตริก 2% w/v เป็นตัวชะ คอมพอสิตสามารถนำไปใช้ดูดซับไอออนปรอทออกจากน้ำเสียจากโรงกลั่นน้ำมันได้ นอกจากนี้ตัวดูดซับที่สังเคราะห์ได้ยังมีสมบัติแม่เหล็กซึ่งเป็นประโยชน์ในการแยกตัวดูดซับออกจากน้ำที่บำบัดแล้วได้ง่าย

สาขาวิชา ปิโตรเคมีและวิทยาศาสตร์พอลิเมอร์ ลายมือชื่อนิสิต.....  
ปีการศึกษา.....2555..... ลายมือชื่อ อ.ที่ปรึกษาวิทยานิพนธ์หลัก.....  
ลายมือชื่อ อ.ที่ปรึกษาวิทยานิพนธ์ร่วม.....



# # 5372369123 : MAJOR PETROCHEMISTRY AND POLYMER SCIENCE

KEYWORD : MERCURY / MCM-48 / MAGNETIC PARTICLES / ADSORPTION

SUMITRA KHONSA-NGA : MAGNETIC NANOPARTICLE-MESOPOROUS SILICA  
MCM-48 COMPOSITES FOR MERCURY(II) ION REMOVAL. ADVISOR: ASST.  
PROF. FUANGFA UNOB, Ph.D., CO-ADVISOR: NUMPON INSIN, Ph.D 65 pp.

A new MCM-48 based magnetic adsorbent containing thiol groups (MP-Fe<sub>2</sub>O<sub>3</sub>@MCM) was prepared and used for Hg(II) ion removal. Surface area of MCM-48,  $\gamma$ -Fe<sub>2</sub>O<sub>3</sub>@MCM-48 and MP-Fe<sub>2</sub>O<sub>3</sub>@MCM-48 were determined to be 941.67, 850.16, 677.58 m<sup>2</sup>/g, respectively. The obtained products were characterized by X-ray diffraction, Fourier transforms infrared spectroscopy, transmission electron microscopy and scanning electron microscopy. Then the adsorption of Hg(II) by MP-Fe<sub>2</sub>O<sub>3</sub>@MCM-48 was investigated in batch method using solid concentration of 0.2 g/L. The effects of solution pH and contact time were also evaluated. The suitable pH for adsorption of Hg(II) was found to 6 and 60 minutes, respectively. The adsorption behavior followed Langmuir isotherm with calculated maximum adsorption capacity of 208.3 mg Hg/g adsorbent. MP-Fe<sub>2</sub>O<sub>3</sub>@MCM-48 could effectively adsorb Hg(II) ions up to 4 cycles of adsorption/regeneration using 1.0 M thiourea in 2 %w/v HNO<sub>3</sub> as eluent. The composite successfully removed Hg(II) from refinery wastewater. In addition, MP-Fe<sub>2</sub>O<sub>3</sub>@MCM-48 provides a magnetic property that is beneficial in the separation of solid from the treated water.

Field of Study : Petrochemistry and Polymer Science Student's Signature.....

Academic Year : .....2012..... Advisor's Signature.....

Co-advisor's Signature.....

## ACKNOWLEDGEMENTS

First of all, I would like to express greatest gratitude to Assistant Professor Dr. Fuangfa Unob, advisor and Dr. Numpon Insin, co-advisor, for kindness, valuable advices and encouragement throughout this research. Not only giving me a useful advice to achieve this research, Assistant Professor Dr. Fuangfa Unob and Dr. Numpon Insin also give me an informal relationship that makes me pleasure.

In addition, this thesis would not have been accomplished without many precious and valuable advice and comments from all my thesis committee, Assistant Professor Dr. Warinthorn Chavasiri, Associate Professor Dr. Wimonrat Trakarnpruk, and Dr. Vuthichai Ervithayasuporn.

For all of my friends in laboratory, the members of Environmental Analysis Research Unit, Mr. Kittipong Sanuwong, Mr. Sakkarin Boontham, Mr.Pheeraphat Niwasanon and Miss Natthaporn Warreewat, I greatly appreciate their kind assistance, generosity and encouragement throughout the course of my research and I would like to thank the members for their help and friendship.

Finally, I would to express my deepest gratitude to my father and my mother for their love and personal supports at all times.

# CONTENTS

	Page
ABSTRACT (THAI).....	iv
ABSTRACT (ENGLISH).....	v
ACKNOWLEDGEMENTS.....	vi
CONTENTS.....	vii
LIST OF TABLES.....	x
LIST OF FIGURES.....	xi
LIST OF SCHEMES.....	xiii
LIST OF ABBREVIATIONS.....	xiv
<b>CHAPTER I INTRODUCTION.....</b>	<b>1</b>
1.1 Statement of the problem.....	1
1.2 Objectives.....	2
1.3 Scopes of this thesis.....	2
<b>CHAPTER II THEORY AND LITERATURE REVIEW.....</b>	<b>3</b>
2.1 Mesoporous materials.....	3
2.1.1 Mobile Crystalline Material (MCM-48).....	3
2.1.2 Synthesis strategies of MCM-48.....	4
2.1.2.1 Principles of the synthesis.....	4
2.1.2.2 Formation mechanism of mesoporous silica.....	5
2.2 Ferrites.....	8
2.2.1 Magnetite.....	9
2.2.2 Maghemite $\gamma$ -Fe <sub>2</sub> O <sub>3</sub> nanoparticles.....	9
2.3 Information about mercury.....	10
2.3.1 Species and toxicology.....	10
2.3.2 Mercury in petroleum.....	11

	<b>Page</b>
2.3.3 Removal of mercury in wastewater.....	11
2.4 Adsorption.....	11
2.4.1 Physisorption.....	12
2.4.2 Chemisorption.....	12
2.4.3 Adsorption isotherm.....	12
2.4.3.1 Langmuir isotherm.....	12
2.4.3.2 Freundlich isotherm.....	13
2.5 Literature reviews.....	13
<b>CHAPTER III EXPERIMENTS.....</b>	<b>18</b>
3.1 Apparatus.....	18
3.2 Chemicals and reagents.....	19
3.2.1 Chemicals.....	19
3.2.2 Preparation of reagents.....	20
3.3 Preparation of MP-Fe <sub>2</sub> O <sub>3</sub> @MCM-48.....	21
3.3.1 The synthesis of MCM-48.....	21
3.3.2 The synthesis of $\gamma$ -Fe <sub>2</sub> O <sub>3</sub> nanoparticles.....	21
3.3.3 Preparation of composite of $\gamma$ -Fe <sub>2</sub> O <sub>3</sub> and MCM-48 ( $\gamma$ -Fe <sub>2</sub> O <sub>3</sub> @MCM-48).....	22
3.3.3.1 The effect of $\gamma$ -Fe <sub>2</sub> O <sub>3</sub> amount.....	22
3.3.3.2 The effect of contact time.....	23
3.4 Functionalization of 3-mercaptopropyl trimethoxysilane onto $\gamma$ -Fe <sub>2</sub> O <sub>3</sub> @MCM-48.....	24
3.5 Characterization of the obtained composite.....	24
3.6 Adsorption study of mercury.....	24
3.6.1 Effect of mercury solution pH.....	25
3.6.2 Effect of adsorption time.....	25
3.6.3 Adsorption isotherms.....	25
3.7 Reuability of the composites.....	26
3.8 Application in real wastewater sample.....	26

	<b>Page</b>
<b>CHAPTER IV RESULTS AND DISCUSSION</b> .....	27
4.1 Characterization .....	33
4.1.1 Characterization by surface area analyzer .....	33
4.2 Characterization of $\gamma$ -Fe <sub>2</sub> O <sub>3</sub> @MCM-48 morphology by SEM and TEM .....	36
4.2.1 Morphology by scanning electron microscopy (SEM)...	36
4.2.2 Morphology by transmission electron microscopy (TEM)	36
4.3 Surface modification with 3-mercaptopropyl trimethoxysilane	38
4.4 Adsorption study .....	40
4.4.1 Preliminary study .....	40
4.4.2 Effect of pH of Hg(II) ions solutions .....	42
4.4.3 Effect of adsorption time .....	43
4.4.4 Adsorption isotherms .....	44
4.5 Reusability of the composites .....	50
4.6 Application in real wastewater samples .....	51
<b>CHAPTER V CONCLUSION</b> .....	52
<b>REFERENCES</b> .....	54
<b>APPENDIX</b> .....	62
<b>VITAE</b> .....	65

## LIST OF TABLES

		Page
Table 2.1	Example of interactions between surfactant and inorganic soluble species .....	4
Table 2.2	Functionalized mesoporous silica for removal of mercury ions	14
Table 3.1	List of characterization and analytical apparatus .....	18
Table 3.2	List of chemicals .....	19
Table 3.3	Detail of heating program in the synthesis of $\gamma$ -Fe <sub>2</sub> O <sub>3</sub> nanoparticles	22
Table 4.1	Amount of $\gamma$ -Fe <sub>2</sub> O <sub>3</sub> nanoparticles observed in $\gamma$ -Fe <sub>2</sub> O <sub>3</sub> @MCM-48 composites.....	31
Table 4.2	Surface area and pore diameter of the materials .....	35
Table 4.3	Adsorption efficiency of MP-Fe <sub>2</sub> O <sub>3</sub> @MCM-48 composites prepared using different amount of $\gamma$ -Fe <sub>2</sub> O <sub>3</sub> .....	40
Table 4.4	The maximum adsorption capacity of the MP-Fe <sub>2</sub> O <sub>3</sub> @MCM-48 compared to other modified mesoporous silica for Hg(II) ions adsorption.....	47
Table 5.1	The adsorption behavior and suitable conditions of the removal of Hg(II) ion .....	52
Table A.1	The observed number of moles of $\gamma$ -Fe <sub>2</sub> O <sub>3</sub> on the composite..	63
Table A.2	The theoretical number of moles of $\gamma$ -Fe <sub>2</sub> O <sub>3</sub> on the composite..	64

## LIST OF FIGURES

	Page
Figure 2.1 Structure of mesoporous M41S materials a) MCM-41, b) MCM-48 and c) MCM-50.....	3
Figure 2.2 Schematic model for the formation of mesoporous silica via two possible pathways a) true liquid crystal template mechanism and b) cooperating liquid template mechanism....	5
Figure 2.3 Phase diagram of CTAB in water.....	6
Figure 2.4 Ternary phase diagram of system $\text{SiO}_2/\text{CTA}^+/\text{H}_2\text{O}$ (H, C and L indicate the predominance areas of the hexagonal, cubic and lamellar structure, respectively.).....	7
Figure 2.5 Cubic MCM-48 mesoporous structure.....	7
Figure 2.6 The two magnetic sublattices A and B of a spinel structure.....	8
Figure 2.7 Comparison of cation distributions in normal spinel and inverse spinel. A and B indicate A sublattice and B sublattice cations, respectively; arrows indicate directions of cationic magnetic moments.....	9
Figure 2.8 Structure of magnetite.....	9
Figure 2.9 Structure of maghemite.....	10
Figure 4.1 X-ray powder diffraction pattern of the as-synthesized MCM-48 compared to JCPDS file No.50-0511 of MCM-48.....	27
Figure 4.2 X-ray powder diffraction pattern of the as-synthesized $\gamma\text{-Fe}_2\text{O}_3$ compared to JCPDS file No.39-1346 of $\gamma\text{-Fe}_2\text{O}_3$ .....	28
Figure 4.3 Low-angle X-ray powder diffraction patterns of MCM-48, 40% $\gamma\text{-Fe}_2\text{O}_3$ @MCM-48 and JCPDS file No.50-0511 of MCM-48	29
Figure 4.4 High-angle X-ray powder diffraction patterns of $\gamma\text{-Fe}_2\text{O}_3$ , $\gamma\text{-Fe}_2\text{O}_3$ @MCM-48 and JCPDS file No.39-1346 of $\gamma\text{-Fe}_2\text{O}_3$ .....	30

	<b>Page</b>	
Figure 4.5	Magnetic properties exhibition of (a) $\gamma$ -Fe <sub>2</sub> O <sub>3</sub> , (b) MP-Fe <sub>2</sub> O <sub>3</sub> @MCM-48 in solution before applying magnetic field and (c) MP-Fe <sub>2</sub> O <sub>3</sub> @MCM-48 in solution after applying magnetic field.....	30
Figure 4.6	Amount of $\gamma$ -Fe <sub>2</sub> O <sub>3</sub> nanoparticles in $\gamma$ -Fe <sub>2</sub> O <sub>3</sub> @MCM-48 prepared by using different contact time between $\gamma$ -Fe <sub>2</sub> O <sub>3</sub> and MCM-48.....	32
Figure 4.7	Isotherm of N <sub>2</sub> adsorption by (a) MCM-48, (b) 40% $\gamma$ -Fe <sub>2</sub> O <sub>3</sub> @MCM-48, (c) 50% $\gamma$ -Fe <sub>2</sub> O <sub>3</sub> @MCM-48, (d) 60% $\gamma$ -Fe <sub>2</sub> O <sub>3</sub> @MCM-48 and (e) 70% $\gamma$ -Fe <sub>2</sub> O <sub>3</sub> @MCM-48.....	33
Figure 4.8	SEM images of 40% $\gamma$ -Fe <sub>2</sub> O <sub>3</sub> @MCM-48 composites with (a) low and (b) high magnifications.....	36
Figure 4.9	TEM images of the as-synthesized MCM-48.....	37
Figure 4.10	TEM images of the as-synthesized $\gamma$ -Fe <sub>2</sub> O <sub>3</sub> with (a) low and (b) high magnifications.....	37
Figure 4.11	TEM images of the 40% $\gamma$ -Fe <sub>2</sub> O <sub>3</sub> @MCM-48 composites with (a) low and (b) high magnifications.....	38
Figure 4.12	FT-IR spectra of (a) MCM-48, (b) $\gamma$ -Fe <sub>2</sub> O <sub>3</sub> @MCM-48 and (c) MP-Fe <sub>2</sub> O <sub>3</sub> @MCM-48.....	39
Figure 4.13	Effect of pH on Hg(II) adsorption on MP-Fe <sub>2</sub> O <sub>3</sub> @MCM-48; initial concentration 40 mg/L; adsorption time 60 minutes.....	42
Figure 4.14	Aqueous speciation diagram of Hg(II) at different solution pH.....	43
Figure 4.15	Effect of adsorption time on Hg(II) adsorption on MP-Fe <sub>2</sub> O <sub>3</sub> @MCM-48; initial concentration 40 mg/L; pH 6.....	44
Figure 4.16	Adsorption isotherm of Hg(II) adsorption on MP-Fe <sub>2</sub> O <sub>3</sub> @MCM-48; pH 6; adsorption time 60 minutes.....	45
Figure 4.17	Linear Langmuir plot of Hg(II) adsorption on MP-Fe <sub>2</sub> O <sub>3</sub> @MCM-48	46
Figure 4.18	Linear Freundlich plot of Hg(II) adsorption on MP-Fe <sub>2</sub> O <sub>3</sub> @MCM-48	47
Figure 4.19	Hg(II) adsorption by MP-Fe <sub>2</sub> O <sub>3</sub> @MCM-48 in sequential uses....	50



## LIST OF SCHEME

	<b>Page</b>
Scheme 4.1    Interaction between $\text{COO}^-$ group of oleic acid and iron atoms.....	38

## LIST OF ABBREVIATIONS

MCM-48	=	Mobil Crystalline Materials- 48
$\gamma\text{-Fe}_2\text{O}_3\text{@MCM-48}$	=	composite of MCM-48 and maghemite nanoparticles
MP	=	3-mercaptopropyl trimethoxysilane
MP- $\text{Fe}_2\text{O}_3\text{@MCM-48}$	=	composite of MCM-48 and maghemite nanoparticles modified with thiol functional group
MPs	=	Magnetic particles
FTIR	=	Fourier transform infrared spectrometer
XRD	=	X-ray diffractometer
SEM	=	Scanning electron microscope
TEM	=	Transmission electron microscope
g	=	Gram
mg	=	Milligram
L	=	Liter
mL	=	Milliliter

# CHAPTER I

## INTRODUCTION

### 1.1 Statement of the problem

Nowadays, heavy metals are widely used in petrochemical industry in Thailand including in the exploration, oil drilling and production process as catalysts and reagents [1], causing contamination and accumulation of heavy metals in the environment [2]. Some heavy metals in water resource, especially mercury are harmful to human life, animals and plants even at low concentration. Mercury can be accumulated in human body and has adverse effects on human health both acute and chronic poisoning after being exposed [3]. The toxicity of mercury includes damaging of brain and other associated functions and potentially causing of death [4]. Therefore, the removal of mercury from wastewater before release to the environment is mandatory.

Several methods for removing of mercury ions from wastewater including adsorption [5], chemical precipitation [6], ion-exchange [7,8], and coprecipitation [9] have been studied. Adsorption is one of the most popular techniques for this purpose due to its simplicity and low operating cost [10]. Some functionalized mesoporous silica e.g. SBA-15 and MCM-41 [11] are used as sorbents for mercury ions adsorption due to their ordered porous structure and their large surface area. However, one of major drawbacks of using mesoporous silica is when they are used in water treatment application; the separation of the solid from water is difficult because of their small particle size. For this reason, adsorbents that have magnetic properties for an easy separation of the solids from water by applying an external magnetic field have been developed.

MCM-48 is an attractive candidate as sorbents since its cubic structure provides 3-dimensional channels and exceptionally high surface area [12,13].  $\gamma\text{-Fe}_2\text{O}_3$  nanoparticles are superparamagnetic materials with great physical and chemical stabilities and low toxicity. This research focuses on the preparation of new composite of MCM-48 and  $\gamma\text{-Fe}_2\text{O}_3$  nanoparticles ( $\gamma\text{-Fe}_2\text{O}_3\text{@MCM-48}$ ) as magnetic adsorbents for Hg(II) ion adsorption.

## 1.2 Objectives

The objectives of this research are listed below.

- (1) To prepare and characterize new magnetic composites ( $\gamma\text{-Fe}_2\text{O}_3\text{@MCM-48}$ ).
- (2) To study the effect of adsorption parameters on Hg(II) adsorption efficiency and apply the adsorbent in the treatment of Hg(II) in wastewater.

## 1.3 Scopes of the thesis

The scope of this research is firstly to prepare MCM-48 and  $\gamma\text{-Fe}_2\text{O}_3$  nanoparticles, then composites of MCM-48 and  $\gamma\text{-Fe}_2\text{O}_3$  nanoparticles ( $\gamma\text{-Fe}_2\text{O}_3\text{@MCM-48}$ ) were synthesized using various quantities of  $\gamma\text{-Fe}_2\text{O}_3$  nanoparticles ranging from 40-80 %w/w.  $\gamma\text{-Fe}_2\text{O}_3\text{@MCM-48}$  was then modified with 3-(mercaptopropyl)-trimethoxysilane (MP). The obtained adsorbents were characterized by X-ray diffraction (XRD), surface area analysis (Brunauer-Emmett-Teller analyzer, BET), scanning electron microscopy (SEM), transmission electron microscopy (TEM) and Fourier transform infrared spectroscopy (FT-IR). In addition, the amount of  $\gamma\text{-Fe}_2\text{O}_3$  in  $\gamma\text{-Fe}_2\text{O}_3\text{@MCM-48}$  was determined by flame atomic absorption spectrometer (FAAS) after acid digestion of the solid.

The MP- $\gamma\text{-Fe}_2\text{O}_3\text{@MCM-48}$  was used as adsorbent in the adsorption of mercury ions in aqueous solution using batch method. Furthermore, effects of pH of mercury ions solution and extraction time on efficiency of mercury adsorption by MP- $\gamma\text{-Fe}_2\text{O}_3\text{@MCM-48}$  were investigated. The adsorption isotherms and reusability of the adsorbents were also studied. Finally, the adsorbent was applied to extract Hg(II) ions in real wastewater. The concentration of mercury ions in solution was determined by a cold vapor atomic absorption spectrometer (CVAAS).

## CHAPTER II

### THEORY AND LITERATURE REVIEW

#### 2.1 Mesoporous materials

Mesoporous materials are one of molecular sieves which have pore diameters between 20 and 200 Å [14]. Ordered mesostructure silica based M41S materials were discovered in 1990s [15]. Mesoporous silica has received an increasing interest in their applications in catalytic processes and environmental cleanup due to their uniform and well defined pore structure [16], large surface area, narrow pore size distribution [17] and fast adsorption kinetics [18-20]. There are three subgroups of mesoporous silica in family of M41S materials with different pore orientations: a hexagonal structure (MCM-41, SBA-15), a cubic structure (MCM-48) and a lamellar structure (MCM-50).

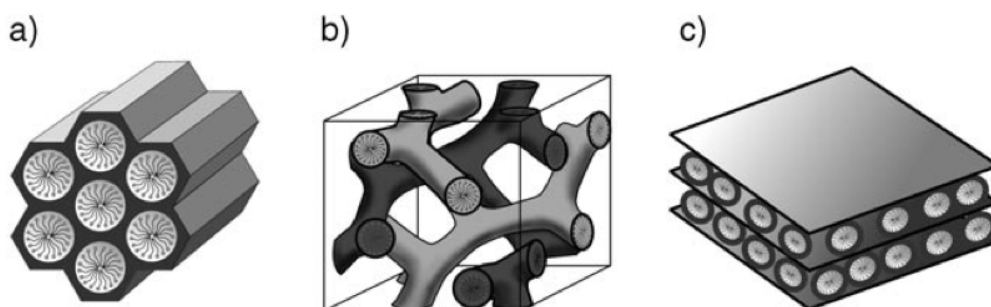


Figure 2.1 Structure of mesoporous M41S materials a) MCM-41, b) MCM-48 and c) MCM-50 [21].

Most of the current researches about the application of mesoporous silica have been focused on MCM-41 and SBA-15 [22-26].

##### 2.1.1 Mobile Crystalline Material-48 (MCM-48)

MCM-48 is mesoporous silica material containing the three dimensional biscontinuous and mesostructure cubic channels indexed in the space group  $la3d$ . In this research, MCM-48 is chosen to be used as adsorbent over MCM-41 and MCM-50 since MCM-48 has three dimensional cubic pore structure while MCM-41 has hexagonal array of unidirectional and non interconnecting pores and MCM-50 has an unstable lamellar structure. The three dimensional channels of MCM-48 provide more favorable mass transfer in catalytic and separation systems than the unidirectional pore system of

MCM-41 [27] and also prevent the pore from being blocked by guest molecules. In addition, specific surface area of MCM-48 is higher than more than that of MCM-41 [28].

## 2.1.2 Synthesis strategies of MCM-48

### 2.1.2.1 Principles of the synthesis

Mesoporous silica is synthesized under mild hydrothermal conditions in the presence of micelles of ionic or non-ionic surfactant under acidic or basic conditions with different silica/surfactant ratios. The synthesis of mesoporous silica requires at least four reagents: solvent (water or alcohol), silica source (tetraethyl orthosilicate (TEOS), tetramethyl orthosilicate (TMOS) or tetrabutyl orthosilicate (TBOS)), surfactant and catalyst. The surfactant micelles are used as a template around which silica framework will form. The mixture is aged at suitable temperature and time. After that, surfactant template is removed by extraction or calcination.

A variety of surfactant types has been used to form mesophases. The surfactant molecules can be categorized based on the properties of their head group and charge as follows:

- Anionic surfactant: the hydrophilic group has a negative charge for example, the alkylchain with sulfate, sulfonate and phosphate groups.
- Cationic surfactant: the hydrophilic group has a positive charge e.g. alkylammonium salts such as, hexadecyltrimethyl ammonium bromide (CTAB).
- Non-ionic surfactant : the hydrophilic group has no charge such as primary amines.

The nature of surfactants and inorganic soluble species interaction is shown in Table 2.1 [15]. , where S is the surfactant, I is the inorganic phase and X and M are the mediating ions.

**Table 2.1** Example of interactions between surfactant and inorganic soluble species

Surfactant type	Inorganic species	Interaction	Example materials
Cationic	$I^-$	$S^+I^-$	MCM-41, MCM-48
	$X^-I^+$	$S^+X^-I^+$	Silica, Zinc phosphate
Anionic	$I^+$	$S^-I^+$	Mg, Al, Ga, Zn oxide
	$M^+I^-$	$S^-M^+I^-$	Zn, Al oxide
Non-ionic	$I^0$	$S^0I^0$	HMS, MSU-X
	$I^+X^-$	$S^0X^-I^+$	SBA-15

For an ionic surfactant ( $S^+$  or  $S^-$ ), the surfactant molecules arrange themselves to form micelles; the hydrophobic tails point toward the center and turn the hydrophilic head outside to bind with inorganic species ( $I^-$  or  $I^+$ ) via electrostatic interaction. The formation routes can be divided into two pathways. In one pathway, inorganic species interact directly with surfactant molecules ( $S^+I^-$  or  $S^-I^+$ ). Another pathway takes place under isoelectric conditions in the presence of counter ions in solution ( $S^+X^-I^+$  or  $S^-M^+I^-$ ). For non-ionic surfactant ( $S^{00}$  or  $S^0X^+I^+$ ), the reaction is done under neutral pH. Interaction between inorganic species and surfactant is hydrogen bonding or dipole-dipole interaction.

### 2.1.2.2 Formation mechanism of mesoporous silica

The formation mechanism of mesoporous silica can be divided into three categories.

- (a) Liquid crystal template mechanism (LCT)
- (b) Folding sheet mechanism [29]
- (c) Hydrogen-bonding interaction [30]

Only LCT mechanism is described in detail in this chapter because MCM-48, which is the mesoporous silica of interest, is formed via this mechanism. LCT mechanism of the formation of MCM-41 structure (Figure 2.2) was often used to explain the LCT mechanism of the first step in the formation of MCM-48 structure.

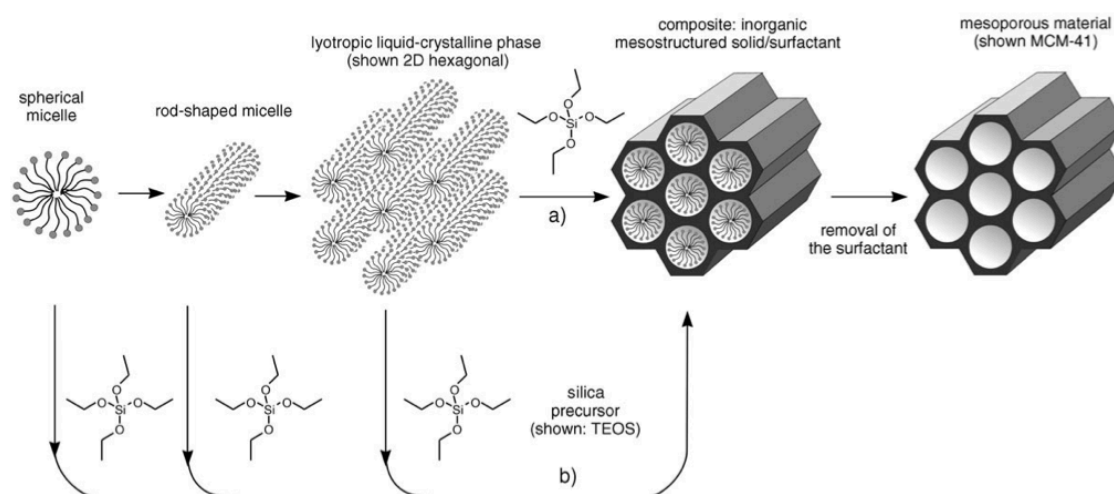


**Figure 2.2** Schematic model for the formation of mesoporous silica via two possible pathways a) liquid crystal template mechanism and b) cooperating liquid template mechanism [21].

There are two possible pathways as shown in Figure 2.2 that are used to synthesize the materials.

- Liquid crystal template mechanism: liquid crystal phase is formed prior to the addition of silicate species.
- Cooperating liquid template mechanism: silicate species are added to the reaction mixture and condensed around micelles.

After silicate framework is formed, the obtained materials are nonporous solid. Thus the surfactant template must be removed to produce the mesoporous materials. The concentration of surfactant can be adjusted to obtain cubic structure (MCM-48) or lamellar structure (MCM-50) [31]. The shape and aggregation of micelles into liquid crystal phase (hexagonal, cubic or lamellar) depending on the concentration of surfactants are shown in phase diagram in Figure 2.3.

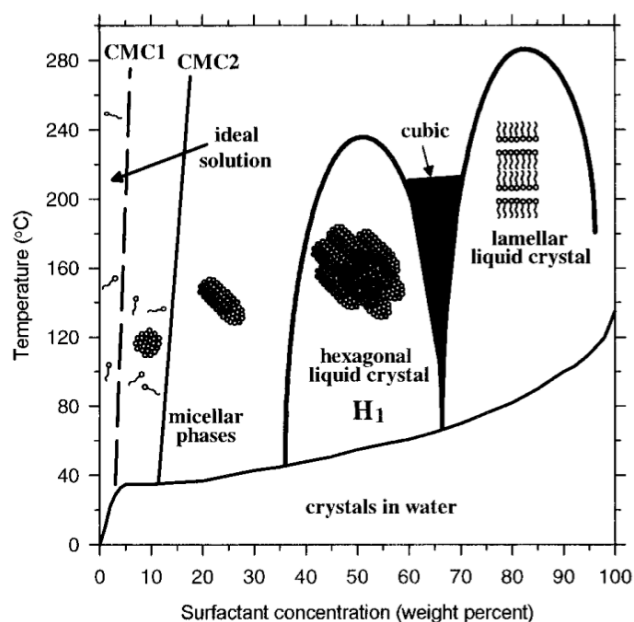
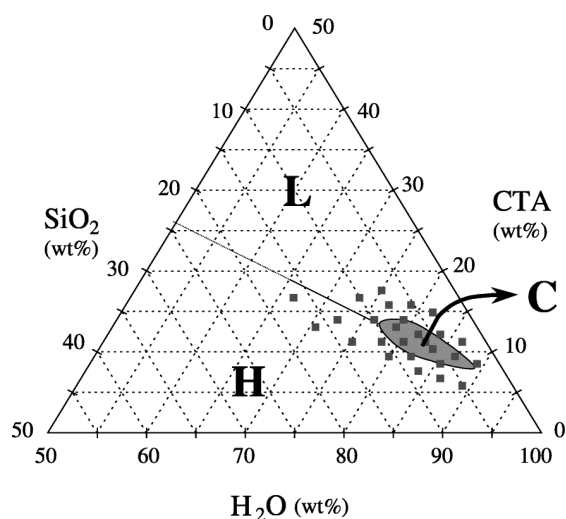


Figure 2.3 Phase diagram of CTAB in water [32].

The role of the surfactant concentrations on the formation of hexagonal, cubic and lamellar structure can be described as follows. At very low surfactant concentration, the surfactants stay as free molecules dissolved in solution. When the surfactant concentration reaches its critical micelle concentration (CMC), small spherical micelles are formed in order to decrease entropy of the system and at higher surfactant concentration, spherical micelles can combine together to form cylindrical micelles.



According to the phase diagram above, the key to form mesoporous silica is the surfactant concentration or molar ratio of surfactant/Si. The primary condition for forming cubic MCM-48 phase is the use of high surfactant/Si ratio to obtain a composition for cubic phase formation in gels synthesis as shown in  $\text{SiO}_2/\text{CTA}^+/\text{H}_2\text{O}$  phase diagram in Figure 2.4.



**Figure 2.4** Ternary phase diagram of  $\text{SiO}_2/\text{CTA}^+/\text{H}_2\text{O}$  system (H, C and L indicate the predominance area of the hexagonal, cubic and lamellar structure, respectively and  $\text{CTA}^+$  is alkylammonium salts) [33].

The difficulties in formation of cubic structure under specific condition might be the reason why MCM-48 has not been widely used. On the other hand, MCM-48 is also attractive for its cubic structure has two independent intertwined channel network (Figure 2.5) which prevent the channels from being blocked by guest molecules.

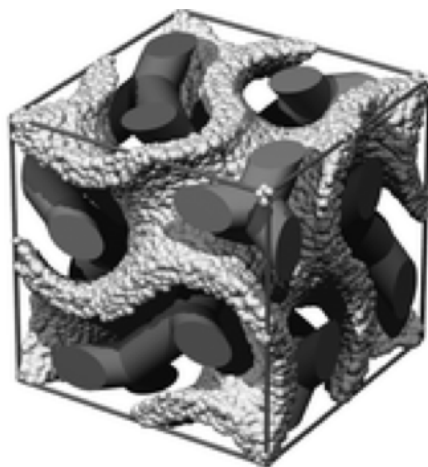


**Figure 2.5** Cubic MCM-48 mesoporous structure [34].

## 2.2 Ferrites [35]

Ferrites are a type of ceramic magnetic nanoparticles contained iron(III) oxide mixed with other metal oxides which have a formula of  $AB_2O_4$  with a cubic spinel structure such as magnetite( $Fe(II)Fe(III)_2O_4$ , or  $Fe_3O_4$ ), cobalt ferrite ( $CoFe_2O_4$ ) and maghemite ( $Fe_2O_3$  with a distorted ferrite structure.) Structure of ferrites contains two cation sites (called A sublattice and B sublattice) separated by oxygen framework as shown in Figure 2.6. Oxygen ions are close-packed in a cubic arrangement and the smaller cations fill in the gaps which classified in the tetrahedral and octahedral sites. The A sublattice is in tetrahedral coordination with 4 surrounding  $O^{2-}$  anions, and there are 8 sites of A sublattice per unit cell. While the B sublattice in octahedral coordinated with 6  $O^{2-}$  anions, and there are 16 sites of B sublattice per unit cell.

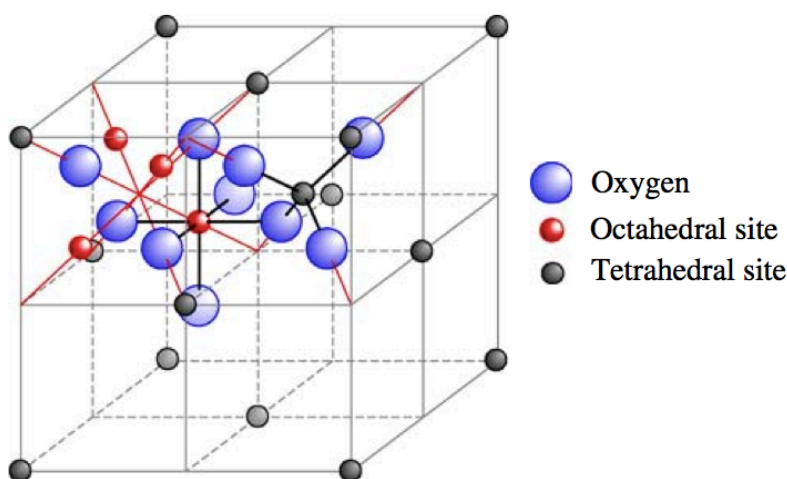


**Figure 2.6** The two magnetic sublattices A and B of a spinel structure [36].

The distribution of divalent and trivalent metals in the A and B sublattices classifies spinel structures into normal spinel and inverse spinel structures. In a normal spinel, similar cations occupy the same sublattice, e.g.  $ZnFe_2O_4$  is a normal spinel with two  $Fe^{3+}$  cations per formula unit occupy B sites and one  $Zn^{2+}$  cation occupies the A sites (Figure 2.7) [37]. Inverse spinel structure possesses different distribution of metals as discussed in the next section.

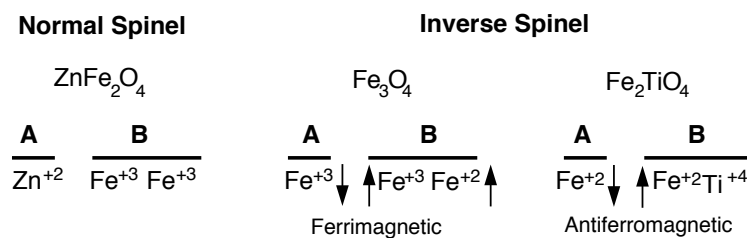


Figure 2.7 Comparison of cation distributions in normal spinel and inverse spinel. A and B indicate A sublattice and B sublattice cations, respectively; arrows indicate directions of cationic magnetic moments.

### 2.2.1 Magnetite [38]

Magnetite ( $Fe_3O_4$ ) has the formula  $(Fe^{3+})^{tet}(Fe^{3+}Fe^{2+})^{oct}O_4$ . A unit cell contains 16  $Fe^{3+}$  and 8  $Fe^{2+}$  cations. Magnetite adopts an inverse spinel structure, of which the two B sites per formula unit are occupied by one of  $Fe^{2+}$  and  $Fe^{3+}$ , and the remaining  $Fe^{3+}$  cations occupies the A sites as shown in Figure 2.8.

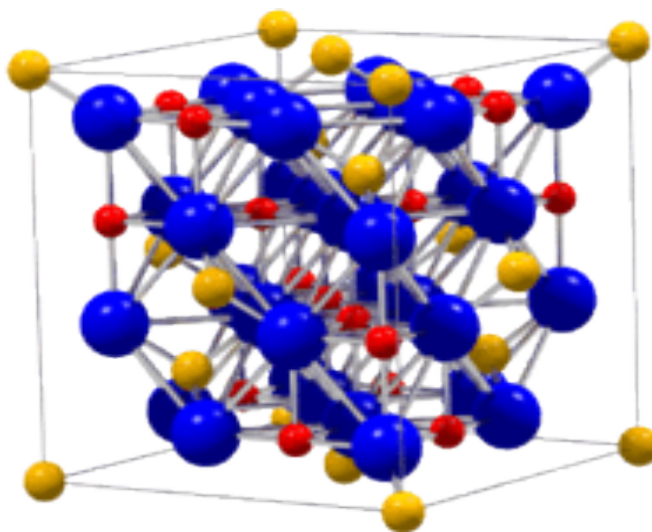


Figure 2.8 Structure of magnetite [39]

### 2.2.2 Maghemite $\gamma$ - $Fe_2O_3$ nanoparticles [40]

The maghemite ( $\gamma$ - $Fe_2O_3$ ) is an inverse spinel magnetic material with a cubic structure. Oxygen ions of maghemite give rise to a cubic close packed structure (ccp) arrays parallel to plain (111) and stacked along the direction (111).

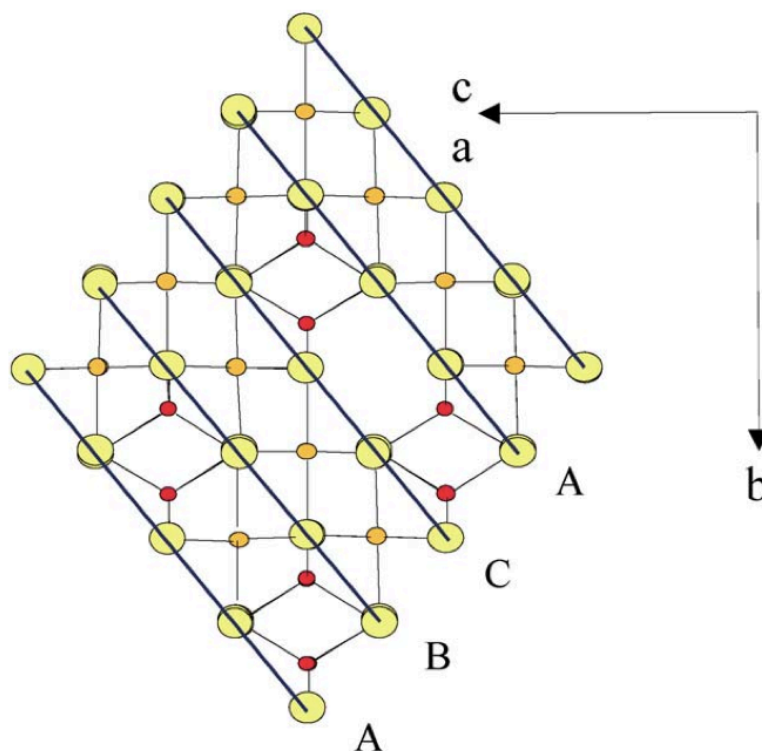


Figure 2.9 Structure of maghemite [40]

Comparing to magnetite ( $\text{Fe}_3\text{O}_4$ ), which presents  $\text{Fe}^{2+}$ ,  $\text{Fe}^{3+}$  ions occupied between tetrahedral and octahedral sites according to the formula  $(\text{Fe}^{3+})^{\text{tet}}(\text{Fe}^{3+}\text{Fe}^{2+})^{\text{oct}}\text{O}_4$ , Maghemite ( $\gamma\text{-Fe}_2\text{O}_3$ ) can be considered as an oxidized magnetite. The formula of maghemite could be  $(\text{Fe}^{3+})^{\text{tet}}(\text{Fe}^{3+}_{5/3}\square_{1/3})^{\text{oct}}\text{O}_4$  where  $\square$  is a vacancy. Maghemite is ferrimagnetic which have superparamagnetic phenomenon which is similar to magnetite. However, maghemite nanoparticles are of our interest in this work because of finite size effects, high stability toward oxidation, and high surface/volume ratios [41].

## 2.3 Information about mercury

### 2.3.1 Species and toxicology

Elemental mercury and mercury compounds are extremely toxic, especially its organometallic forms. Elemental mercury ( $\text{Hg}^0$ ) is the major species of mercury in atmosphere which can be absorbed into the human blood stream.  $\text{Hg}^0$  can be oxidized

to  $\text{Hg}^+$ ,  $\text{Hg}^{2+}$  species and form compounds. The most toxic species are organic-mercury compounds such as methyl and dimethyl mercury.

### 2.3.2 Mercury in petroleum [42]

In petroleum industry, mercury is found in crude oil, natural gas, condensates, wastewater and soil around platform in various forms i.e. elemental, ionic and organometallic. Elemental mercury is almost found in natural gas whereas organic-mercury compounds are found in condensates and petroleum liquids. The more using of petrochemical products the more emission of mercury to environment was observed. Mercury from petroleum industry enters the environment via drilling process, combustion of fuels and release of waste or wastewater.

### 2.3.3 Removal of mercury in wastewater

Mercury in wastewater could be removed by several methods as follows:

- Adsorption
- Chemical precipitation
- Co-precipitation
- Reduction processes
- Ion exchange

Adsorption is one of the most popular techniques due to its simplicity and low operating cost [43].

## 2.4 Adsorption [44]

Adsorption is the phenomenon of the sorption that takes place between liquid or gas phase and solid phase. The target analytes in liquid or gas phase (called adsorbate) are attracted to the surface of solid phase (called adsorbent) via mass transfer. The adsorption can be divided into two types; physisorption and chemisorption.

### 2.4.1 Physisorption

Physisorption is a process in which adsorbed atoms or molecules interact with surfaces via weak van der Waals force. The adsorbates are increasingly adsorbed on surface in multilayer regime and the number of layers depends on concentration of adsorbate. The adsorbed atoms or molecules can freely move over surface and the sorption system is reversible which reversibility depends on strength of interaction between adsorbate and adsorbent.

### 2.4.2 Chemisorption

Chemisorption takes place through chemical reaction between adsorbate and adsorbent. Interaction between adsorbate and adsorbent (i.e. ionic and covalent bond) is stronger than van der Waals force and it is irreversible system. The adsorbates occupy specific active site on surface of adsorbent and form monolayer adsorption.

### 2.4.3 Adsorption isotherm

In the adsorption process, adsorption of adsorbate on adsorbent surface at thermodynamic equilibrium and constant temperature is called adsorption isotherm. Several isotherm models including Langmuir and Freundlich model are widely used to describe the relationship between adsorbate and adsorbent at equilibrium [45].

#### 2.4.3.1 Langmuir isotherm

Langmuir isotherm model was proposed based on the assumption that adsorbates are adsorbed via monolayer chemisorption onto the homogenous surface of adsorbent at constant temperature. The Langmuir equation is shown in Eq. 2.1 and can be rearranged in to linear equation form as shown in Eq. 2.2;

$$q_e = \frac{b q_m C_e}{1 + b C_e} \quad (2.1)$$

$$\frac{C_e}{q} = \frac{1}{q_m b} + \frac{C_e}{q_m} \quad (2.2)$$

where  $q_e$  = amount of target analyte adsorbed at equilibrium (mg/g)  
 $C_e$  = equilibrium concentration of adsorbate in bulk solution (mg/g)  
 $q_m$  = maximum adsorption capacity of adsorbent (mg/g)  
 $b$  = Langmuir constant related to affinity of binding sites (L/mg)

A plotting  $C_e/q_e$  versus  $C_e$ , gives a strain line with a slope and intercept of  $1/q_m$  and  $1/bq_m$ , respectively [46].

#### 2.4.3.2 Freundlich isotherm

Freundlich isotherm model have assumption that adsorbate are adsorbed via multilayer adsorption onto heterogeneous surface of adsorbent. The Freundlich equation is shown in Eq. 2.3 and the linear form is shown in Eq. 2.4;

$$q_e = K_f C_e^{1/n} \quad (2.3)$$

$$\ln q_e = \ln K_f + \frac{1}{n} \ln C_e \quad (2.4)$$

where  $K_f$  = Freundlich constant related to adsorption capacity of adsorbent (mg/g)  
 $n$  = Freundlich constant related to adsorption intensity

A plotting  $\ln q_e$  versus  $\ln K_f$ , gives a slope and intercept of  $\frac{1}{n}$  and  $\ln K_f$  respectively, [46].

## 2.5 Literature reviews

Some mesoporous silica has been widely used in adsorption system for removal of mercury and other heavy metals due to their beneficial properties especially, large surface area. Surface of mesoporous silica was modified with various functional groups e.g. functional groups containing sulfur atom, in order to improve the selectivity and affinity toward mercury ions. The efficiency of mesoporous silica modified by various functional groups in removal of mercury are compared in the following table.

Table 2.2 Functionalized mesoporous silica for removal of mercury ions

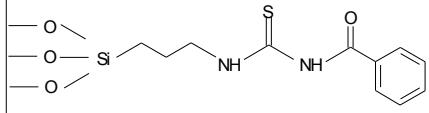
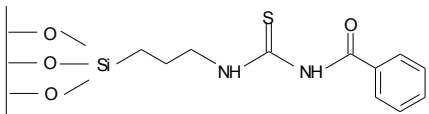
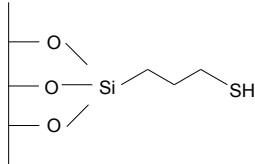
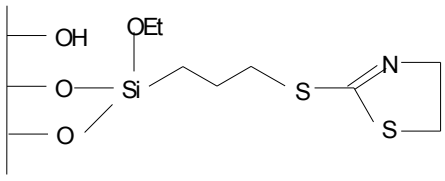
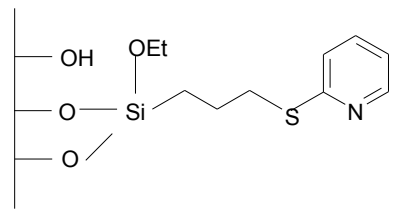
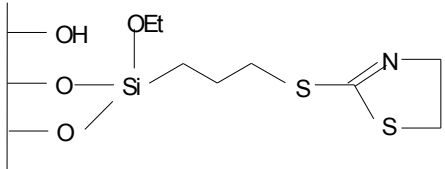
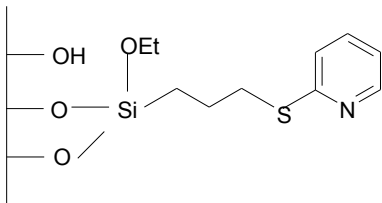
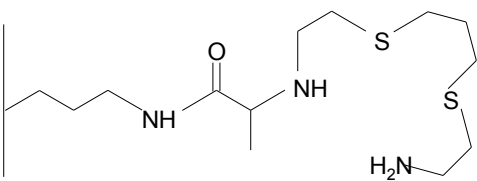
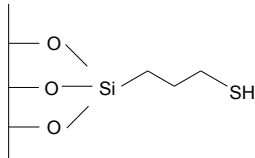
Adsorbent	Modified surfaces	Adsorption capacity (mmol/g)	Reference
MCM-41	 <p>Benzoylthiourea</p>	5.00	[47]
MCM-48	 <p>Benzoylthiourea</p>	1.55	[48]
SBA-15	 <p>3-mercaptopropyltrimethoxysilane</p>	0.40	[49]
SBA-15	 <p>2-mercaptothiazoline</p>	1.10	[50]
SBA-15	 <p>2-mercaptopyridine</p>	0.16	[51]



Table 2.2 Functionalized mesoporous silica for removal of mercury ions (continued)

Adsorbent	Ligand	Adsorption capacity (mmol/g)	Reference
MCM-41	 2-mercaptothiazoline	0.70	[50]
MCM-41	 2-mercaptopyridine	0.12	[51]
MCM-41	 2-(3-(2-aminoethylthio)propylthio)ethanamine	0.79	[52]
MCM-48	 3-mercaptopropyltrimethoxysilane	2.20	[12]

According to the table above, MCM-48 could adsorb mercury ions with higher adsorption capacity than others mesoporous silica (e.g. MCM-41 and SBA-15). When mesoporous silica is used in water treatment, the users may encounter some difficulties in the separation of solid from water because of their small particle sizes. For this reason, development of MCM-48 adsorbents that have magnetic properties for easy

separation of the solid from solution by applying an external magnetic field is studied in this work.

There are several researches reporting the synthesis of mesoporous silica and magnetic nanoparticles composites for the use in various applications as shown as follows.

Kolotilova *et al.* [53] synthesized composites of MCM-41 and  $\text{Fe}_3\text{O}_4$  for used as molecular sieve by introduction of  $\text{Fe}_3\text{O}_4$  nanoparticles in CTAB solution during the synthesis of MCM-41. Results from TEM, SEM and X-ray diffraction were used to confirm the incorporation of  $\text{Fe}_3\text{O}_4$  nanoparticles in MCM-41. The  $\text{Fe}_3\text{O}_4$  nanoparticles were captured in porous silica matrix of MCM-41. Surface area of the composites was in a range of 392 to 366  $\text{m}^2/\text{g}$  depending on the content of  $\text{Fe}_3\text{O}_4$ .

Emamian *et al.* [54] synthesized and characterized MCM-41/ $\text{CoFe}_2\text{O}_4$  nanocomposites via impregnation of Co-Fe complex solution in mesoporous MCM-41 matrix under reduced pressure. The phase composition morphology was investigated by TEM and it was observed that cobalt ferrite phase was formed within the mesoporous silica channels.

Chen *et al.* [55] synthesized magnetic MCM-41 using  $\text{Fe}_3\text{O}_4$  as magnetic nanoparticles for removal of Cr(VI). The magnetic composite could be obtained by adding colloidal suspension of magnetic  $\text{Fe}_3\text{O}_4$  nanoparticles into a solution of CTAB and  $\text{HN}_4\text{OH}$  during the synthesis of MCM-41. The results from TEM showed that  $\text{Fe}_3\text{O}_4$  was encapsulated in MCM-41 and the surface area of obtained magnetic MCM-41 materials was around 550  $\text{m}^2/\text{g}$ .

Kima *et al.* [56] prepared magnetic SBA-15 for removal of mercury ions in wastewater.  $\text{Fe}(\text{NO}_3)_3 \cdot 9\text{H}_2\text{O}$  treated with propionic acid vapor was impregnated into SBA-15 before decomposition of iron propionate complex to produce magnetic SBA-15 composites. It was found that magnetic nanoparticles were formed outside the pores of SBA-15.

Rosenholm *et al.* [57] proposed the synthesis of mesoporous silica-magnetite ( $\text{Fe}_3\text{O}_4$ ) nanocomposites by coating of SBA-15 on magnetite cores for using in

biomedical applications. The obtained materials represented the core-shell system where uniform mesoporous shell was produced around the magnetite particle.

Qiang *et al.* [58] synthesized magnetic mesoporous nanocomposites (FeM48) using  $\text{Fe}_3\text{O}_4$  as magnetic particles and applied the material to remove sulfamethazine (SMN) from water. The synthesis was performed by adding  $\text{Fe}_3\text{O}_4$  nanoparticles into a solution of 1 $\text{SiO}_2$ : 0.15CTAB: 0.02Sodium laurites: 0.5NaOH: 58 $\text{H}_2\text{O}$  during the synthesis of MCM-48. The TEM images of the obtained MCM-48 and  $\text{Fe}_3\text{O}_4$  composite showed that the inner core  $\text{Fe}_3\text{O}_4$  was coated with an outer shell of MCM-48.

Most of the methods for synthesis of mesoporous silica and magnetic nanoparticles composites are focused on coating of mesoporous silica on magnetic particles or impregnation of magnetic complex into pore system of mesoporous silica. All those methods require suitable conditions such as chemical precursors and many steps in the synthesis. This work proposes a simple way to synthesize the mesoporous silica MCM-48 and maghemite composites. Monodisperse magnetic nanoparticles in solvent were mixed together with mesoporous silica followed by evaporation of solvent to produce the magnetic mesoporous silica composites.

## CHAPTER III

### EXPERIMENTS

In this work, magnetic composite of MCM-48 modified with 3-mercaptopropyl trimethoxysilane (MP-Fe<sub>2</sub>O<sub>3</sub>@MCM-48) was prepared and used as adsorbent for removal of mercury ions. The experimental is divided into two parts.

Part I: Preparation of MP-Fe<sub>2</sub>O<sub>3</sub>@MCM-48 including

- The synthesis of MCM-48
- The synthesis of  $\gamma$ -Fe<sub>2</sub>O<sub>3</sub> nanoparticles
- Preparation of composite of  $\gamma$ -Fe<sub>2</sub>O<sub>3</sub> and MCM-48 ( $\gamma$ -Fe<sub>2</sub>O<sub>3</sub>@MCM-48) by
  - The effect of  $\gamma$ -Fe<sub>2</sub>O<sub>3</sub> amount
  - The effect of contact time
- Functionalization of 3-mercaptopropyl trimethoxysilane onto  $\gamma$ -Fe<sub>2</sub>O<sub>3</sub>@MCM-48
- Characterization of the obtained composites

Part II: Adsorption study of mercury including

- Effect of mercury solution pH
- Effect of adsorption time
- Adsorption isotherms
- Reusability of the composites
- Application in real wastewater samples

The apparatus and chemicals used are given in Table 3.1.

#### 3.1 Apparatus

Table 3.1 List of characterization and analytical apparatus

Apparatus	Model
X-ray diffraction spectrometer (XRD)	DMAX 2200/Ultima <sup>+</sup> (Rigaku)
Surface area analyzer	BELSORP-mini (BEL Japan)
Transmission electron microscope (TEM)	JEM-2100 (JOEL)

**Table 3.1** List of characterization and analytical apparatus (continued)

Apparatus	Model
Scanning electron microscope (SEM)	JSM-5410LV (JOEL)
Fourier transform infrared spectrometer (FT-IR)	Impact 410 (Nicolet)
Cold vapor atomic absorption spectrometer (CVAAS)	Analyst 100 coupled with FIAS400 system (Perkin-Elmer)
Flame atomic absorption spectrometer (FAAS)	Analyst 100 (Perkin-Elmer)
Centrifuge	Centaur 2 (Sanyo)
pH meter	pH 211 (Hanna instrument)
Rotary evaporator	N-1000 (Eyela)
Stirrer	MS 101 (Gem)

### 3.2 Chemicals and reagents

#### 3.2.1 Chemicals

All chemicals listed in Table 3.2 are reagent grade and used without further purification.

**Table 3.2** List of chemicals

Chemicals	Suppliers
Hexadecyltrimethyl ammonium bromide (CTAB)	Fluka
Sodium hydroxide	Merck (99%)
Tetraethoxysilane (TEOS)	Aldrich (reagent 98%)
Hydrochloric acid conc.	Merck
Ethanol	Merck
Iron (III) chloride ( $\text{FeCl}_3$ )	Fisher Scientific
Oleic acid	Merck
n-Hexane	CarLo Eaba
1-Ocadecene	Aldrich (technical grade, 90%)
Nitric acid conc.	Merck

Table 3.2 List of chemicals (continued)

Chemicals	Suppliers
3-(Mercaptopropyl)-trimethoxysilane (MP)	Aldrich
Toluene	Merck (99.9%)
Sodium nitrate	Fluka (>99.0%)
Mercury (II) standard solution (1000 mg/L)	Fluka (For AAS)
Iron (III) standard solution (1000 mg/L)	Merck
Hydrogen peroxide	Merck (for synthesis)
Stannous chloride	Fluka
Thiourea	Sigma-Aldrich

### 3.2.2 Preparation of reagents

All reagents were prepared using de-ionized water.

Mercury solutions: Mercury standard solution (1000 mg/L) was used to prepare the mercury solutions of required concentrations.

Sodium nitrate solutions: Sodium nitrate solution (0.01 M) used to control the solution ionic strength was prepared daily by dissolving an appropriate amount of  $\text{NaNO}_3$  in de-ionized water.

Sodium hydroxide solutions: Sodium hydroxide solutions (1, 5 and 10 %w/v) used for pH adjustment were prepared daily by dissolving an appropriate amount of NaOH in de-ionized water.

Nitric acid solutions: Nitric acid solutions (1, 5 and 10 %v/v and 6M) for pH adjustment and composite washing were prepared daily by direct dilution of the concentrated acid solution (65 %).

Hydrochloric acid solutions: Hydrochloric acid solutions (3 %v/v) used as acid carrier in Hg(II) determination by cold vapor atomic absorption spectrometer were prepared daily by direct dilution of the concentrated acid solution (37 %).

Tin (II) chloride solutions: Tin (II) solutions were prepared and used as reducing reagent for Hg(II) determination by cold vapor atomic absorption spectrometer. Ten grams of  $\text{SnCl}_2$  were dissolved in 700 mL of de-ionized water. Then 80 mL of HCl 37% (v/v) was added, the volume was adjusted to 1000 mL with de-ionized water.

Potassium permanganate solution: 5% w/v of potassium permanganate solution was prepared by dissolving 5 g of  $\text{KMnO}_4$  in 100 mL of de-ionized water.

Potassium persulfate solution: 5% w/v of potassium persulfate solution was prepared by dissolving 5 g of  $\text{K}_2\text{S}_2\text{O}_8$  in 100 mL of de-ionized water.

Sodium chloride-hydroxylammonium hydrochloride solution: 12 g  $\text{NaCl}$  and 12 g  $\text{NH}_2\text{OH}\cdot\text{HCl}$  were dissolved in 100 mL of de-ionized water.

### 3.3 Preparation of $\text{MP-Fe}_2\text{O}_3@\text{MCM-48}$

#### 3.3.1 The synthesis of MCM-48

MCM-48 material was synthesized by following a method described by Gies et al [59] with some modification. Tetraethoxysilane (TEOS) and hexadecyltrimethyl ammonium bromide (CTAB) were used as silica source and surfactant template, respectively. The synthesis mixture having molar composition of  $1(\text{TEOS}):0.7(\text{CTAB}):0.5(\text{NaOH}):64\text{H}_2\text{O}$  was prepared.  $\text{NaOH}$  was dissolved in a HDPE bottle and then aqueous CTAB solution was slowly dropped to  $\text{NaOH}$  solution under continuous stirring and stirred for 15 min. TEOS was then added drop-wise and the mixture was stirred and heated at  $40\text{-}50\text{ }^\circ\text{C}$  for 3 h. The milky solution was crystallized at  $90\text{ }^\circ\text{C}$  in an oven for 4 days to give MCM-48. The obtained solid was washed with de-ionized water and dried at the room temperature overnight. Then solid was washed again with a solution of water, ethanol and  $\text{HCl}$  in molar ratio of  $90:5:10$  to neutralise the solid and dried at room temperature. After purification, white powder was obtained and calcined at  $540\text{ }^\circ\text{C}$  for 5 h to remove the template.

#### 3.3.2 The synthesis of $\gamma\text{-Fe}_2\text{O}_3$ nanoparticles

Monodisperse  $\gamma\text{-Fe}_2\text{O}_3$  nanoparticles were synthesized by following the method described by Park et al [60]. Iron-oleate complex was first prepared as follows. Sodium oleate (24 mmol) and  $\text{FeCl}_3$  (8 mmol) were dissolved in mixed solvent containing 16 mL of ethanol, 12 mL of de-ionized water and 28 mL of hexane. The mixture was refluxed at  $70\text{ }^\circ\text{C}$  for 4 h and two layers solution were observed after refluxing. Iron-oleate in upper organic layer was washed three times in a separation funnel with 6 mL de-ionized water. Hexane in this phase was removed by evaporation, and consequently iron-oleate complex in a waxy solid form was obtained. Monodisperse  $\gamma\text{-Fe}_2\text{O}_3$  nanoparticles were

further synthesized as follows. Iron-oleate complex (8 mmol) and oleic acid (4 mmol) were added to 20 g of 1-octadecene. The mixture was slowly heated to 320 °C with a rate of 3.3 °C /min and maintained at 320 °C for 30 min to age and generate iron oxide nanocrystals using a temperature controller. The detail in heating program for the synthesis of  $\gamma$ -Fe<sub>2</sub>O<sub>3</sub> nanoparticles is shown in table 3.3.

**Table 3.3** Detail of heating program in the synthesis of  $\gamma$ -Fe<sub>2</sub>O<sub>3</sub> nanoparticles

Step	Temperature profile	Time profile	Note
1	50 °C	15 min	-
2	50 °C	60 min	-
3	320 °C	81 min	Feed N <sub>2</sub> at 100 °C
4	320 °C	30 min	-
5	160 °C	5 min	-
6	160 °C	120 min	Feed O <sub>2</sub>
7	50 °C	30 min	-

After heating, the solution became brownish-black and turbid, containing nanocrystals. The mixture was cooled to room temperature. The nanocrystals were precipitated using ethanol and separated out of mixture via centrifugation.

### 3.3.3 Preparation of composite of $\gamma$ -Fe<sub>2</sub>O<sub>3</sub> and MCM-48 ( $\gamma$ -FeO<sub>3</sub> @MCM-48)

#### 3.3.3.1 The effect of $\gamma$ -Fe<sub>2</sub>O<sub>3</sub> amount

Various quantities of  $\gamma$ -Fe<sub>2</sub>O<sub>3</sub> nanoparticles ranging from 40 to 80 percent of MCM-48 weight were used to determine a suitable quantity of  $\gamma$ -Fe<sub>2</sub>O<sub>3</sub> nanoparticles for composites synthesis.  $\gamma$ -Fe<sub>2</sub>O<sub>3</sub> nanoparticles dispersed in hexane of the studied quantity were added to the as synthesized MCM-48 and then the mixture was stirred for 4 h at room temperature. Hexane in this mixture was evaporated leaving  $\gamma$ -Fe<sub>2</sub>O<sub>3</sub>@MCM-48 composites as a brown solid. The solid was washed with hexane and 6M HNO<sub>3</sub> solution and dried overnight.

To determine the content of  $\gamma$ -Fe<sub>2</sub>O<sub>3</sub> in the final composites, the magnetic particles attached in composite was extracted. 50 mL of nitric acid and hydrochloric acid in volume ratio of 1:3 was added to 10 mg of  $\gamma$ -Fe<sub>2</sub>O<sub>3</sub>@MCM-48, the mixture was heated at 90-95 °C until there were no more brown fumes. The mixture was further heated until



almost dry. Then, the standard method for digestion of sediment, sludges, and soils (EPA Method 3050B) [61] was used to extract Fe ions from  $\gamma\text{-Fe}_2\text{O}_3\text{@MCM-48}$  as follows;

- 1) 5 mL of 1:1 (v/v)  $\text{HNO}_3$  solution was added to the mixture with continuous heating at 90-95 °C for 15 min.
- 2) 2.5 mL of conc. $\text{HNO}_3$  was added and the mixture was heated for 30 min. This step was repeated again.
- 3) The mixture was heated until total volume was around 5 mL and then cooled down.
- 4) 2 mL of de-ionized water and 3 mL of 30%  $\text{H}_2\text{O}_2$  were added to the mixture and heated gently to prevent the mixture from boiling over.
- 5) 1 mL of 30%  $\text{H}_2\text{O}_2$  was added to the mixture each time and total volume of 30%  $\text{H}_2\text{O}_2$  was 7 mL.
- 6) 2.5 mL of conc. $\text{HCl}$  and 5 mL of de-ionized water were added. The mixture was heated to reflux for 15 min and then, cooled down.
- 7) Dilute and make up the volume of the mixture to 100.00 mL with de-ionized water.
- 8) The mixture was filtered using membrane filter, solution containing Fe ions was obtained.

Concentrations of Fe ions in the solution were determined by flame atomic absorption spectrometer (FAAS).

### 3.3.3.2 The effect of contact time

The effect of contact time between  $\gamma\text{-Fe}_2\text{O}_3$  and MCM-48 in the synthesis of  $\gamma\text{-Fe}_2\text{O}_3\text{@MCM-48}$  was studied using contact time varied from 1 to 5 h.  $\gamma\text{-Fe}_2\text{O}_3$  nanoparticles of desired amount dispersed in hexane were added to the as synthesized MCM-48 and the mixture was stirred for 1, 2, 3, 4 or 5 h at room temperature. Hexane in this mixture was evaporated to obtain  $\gamma\text{-Fe}_2\text{O}_3\text{@MCM-48}$  composites in a brown solid form. The solid was washed with hexane and 6M  $\text{HNO}_3$  solution and dried overnight. Then the content of  $\gamma\text{-Fe}_2\text{O}_3$  in the obtained composites was determined by acid extraction according to the methods described in previous experiment followed by the analysis by FAAS. From the experiment 3.3.3.1 and 3.3.3.2, suitable amount of  $\gamma\text{-Fe}_2\text{O}_3$  and contact time were further applied to the synthesis of  $\gamma\text{-Fe}_2\text{O}_3\text{@MCM-48}$ .

### 3.4 Functionalization of 3-mercaptopropyl trimethoxysilane onto $\gamma$ -Fe<sub>2</sub>O<sub>3</sub>@MCM-48

One gram of  $\gamma$ -Fe<sub>2</sub>O<sub>3</sub>@MCM-48 was immersed in 60 mL of dried toluene and MP was added with a ratio of 20 mmol of MP : 1 g of  $\gamma$ -Fe<sub>2</sub>O<sub>3</sub>@MCM-48. The suspension was refluxed at 110 °C under nitrogen atmosphere for 5 h. After refluxing, the solid was separated by external permanent magnet. The solid was washed with 100 mL of ethanol and dried at 120 °C overnight to yield mercaptopropyl-functionalized  $\gamma$ -Fe<sub>2</sub>O<sub>3</sub>@MCM-48 (MP-Fe<sub>2</sub>O<sub>3</sub>@MCM-48).

### 3.5 Characterization of the obtained composites

The crystalline structure of as synthesized MCM-48,  $\gamma$ -Fe<sub>2</sub>O<sub>3</sub> and  $\gamma$ -Fe<sub>2</sub>O<sub>3</sub>@MCM-48 were confirmed by X-ray diffraction spectrometry (XRD). The XRD pattern of MCM-48 and  $\gamma$ -Fe<sub>2</sub>O<sub>3</sub> were recorded at  $2\theta$  in a range of 1.5 to 8° and 20 to 70°, respectively.

Surface area analyzer was used to determine the surface area and pore diameter of as synthesized MCM-48,  $\gamma$ -Fe<sub>2</sub>O<sub>3</sub>@MCM-48 and MP-Fe<sub>2</sub>O<sub>3</sub>@MCM-48.

Fourier transforms infrared spectrometry (FT-IR) was used to confirm the functional group on MCM-48,  $\gamma$ -Fe<sub>2</sub>O<sub>3</sub>@MCM-48 and MP-Fe<sub>2</sub>O<sub>3</sub>@MCM-48.

Transmission electron microscope (TEM) and scanning electron microscope (SEM) were used to study the morphology of as synthesized MCM-48,  $\gamma$ -Fe<sub>2</sub>O<sub>3</sub> and  $\gamma$ -Fe<sub>2</sub>O<sub>3</sub>@MCM-48.

### 3.6 Adsorption study of mercury

The effect of various parameters that may have influence on Hg(II) adsorption by the composites were studied. 0.01 M NaNO<sub>3</sub> solution was used to control the ionic strength of solution. All batch adsorption experiments were performed by using 5 mg of adsorbent MP-Fe<sub>2</sub>O<sub>3</sub>@MCM-48 and 25.0 mL of 40 mg/L mercury ions solution. The mixture was stirred for a specific duration. The solid was separated from solution using a permanent magnet and the residual concentration of mercury ions in the solution were determined by cold vapor atomic absorption spectrometer. The removal efficiency, R (%) and the amount of Hg(II) adsorbed, q (mg/g) were calculated according to Eq. (3.1) and (3.2), respectively;

$$R = \frac{C_0 - C}{C_0} \times 100 \quad (3.1)$$

$$q = \left( \frac{C_0 - C}{w} \right) V \quad (3.2)$$

where  $C_0$  is the initial concentration,  $C$  is the final concentration of Hg(II) ions in mg/L,  $V$  is the solution volume in litre and  $w$  is the weight in gram of MP-Fe<sub>2</sub>O<sub>3</sub>@MCM-48.

### 3.6.1 Effect of mercury solution pH

The effect of Hg(II) solution pH on removal efficiency was studied in the pH range of 1.0 to 6.0. Solution of 1% HNO<sub>3</sub>, 5% HNO<sub>3</sub>, 10% HNO<sub>3</sub>, 1% NaOH, 5% NaOH or 10% NaOH were used to adjust pH of Hg(II) ions solution (40 mg/L). The contact time in this experiment was 1 h.

### 3.6.2 Effect of adsorption time

The effect of adsorption time on Hg(II) removal efficiency of adsorbent was studied using contact time varied from 5 to 60 min. The pH of Hg(II) solutions (40 mg/L) was adjusted to a desired value.

### 3.6.3 Adsorption isotherms

The adsorption isotherm experiments were performed at 25 °C. The initial concentration of Hg(II) solution was varied in the range of 40 to 400 mg/L. The adsorption of Hg(II) was carried out under the chosen condition i.e. solution pH and contact time to ensure that the adsorption equilibrium was attained. The experimental data were fitted to Langmuir and Freundlich isotherm model to study adsorption behavior.

### 3.7 Reusability of the composites

The reusability was studied by using the same adsorbent in repeated adsorption/regeneration cycles. In adsorption step, MP-Fe<sub>2</sub>O<sub>3</sub>@MCM-48 was used to remove Hg(II) in 25 mL solution containing 50 mg/L Hg(II) ions at pH 6. The adsorption time used was 1 hour. The mixture was centrifuged to separate the adsorbent from residual solution. Hg(II) concentration in residual solution was determined by CVAAS. Then 10 mL of 1.0 M thiourea in 2% W/V HCl was added to the used adsorbent and stirred for 1 hour, thiourea solution was separated from the used adsorbent by centrifugation. The adsorbent was washed twice with DI water and used in another adsorption experiment. The adsorption/regeneration cycle was repeated for 7 times.

### 3.8 Application in real wastewater samples

Wastewater containing mercury collected from a refinery plant (Bangkok) was used to evaluate the adsorption efficiency of MP-Fe<sub>2</sub>O<sub>3</sub>@MCM-48. The wastewater sample was filtered and digested by following the standard method (EPA ASTM3223) [62] in order to convert mercury in sample to mercuric ions before adsorption and determination by CVAAS. The digestion method (ASTM3223) is described as follows.

- 1) 100 mL of filtered wastewater sample was transferred to 250 mL flask.
- 2) 5 mL of concentrated sulfuric acid and 0.25 mL of concentrated nitric acid were added under continuous stirring.
- 3) 10 mL of 5% w/v potassium permanganate (KMnO<sub>4</sub>) solution was added, the solution was stirred. More volume of KMnO<sub>4</sub> solution could be added until the purple color persists.
- 4) 8 mL of 5% w/v potassium persulfate solution was added. The solution was heated using water bath at 95 °C or 2 hours.
- 5) The solution was cooled and then sodium chloride-hydroxylammonium chloride solution was added to reduce the excess amount of permanganate until the solution was transparent. The concentration of mercury in the obtained solution was then determined.

## CHAPTER IV

### RESULTS AND DISCUSSION

In this work, a composite of MCM-48 and  $\gamma\text{-Fe}_2\text{O}_3$  nanoparticles ( $\gamma\text{-Fe}_2\text{O}_3\text{@MCM-48}$ ) was synthesized to produce a magnetic adsorbent that can be easily separated from water by applying an external magnetic field. Then the surface of  $\gamma\text{-Fe}_2\text{O}_3\text{@MCM-48}$  composite was functionalized with (3-mercaptopropyl)trimethoxysilane to obtain  $\text{MP-Fe}_2\text{O}_3\text{@MCM-48}$  for improving efficiency in mercury ions removal.

#### Part I Preparation and characterization of $\text{MP-Fe}_2\text{O}_3\text{@MCM-48}$ adsorbent

Firstly, X-ray diffraction spectroscopy was used to characterize and confirm the crystal structure of the as-synthesized MCM-48,  $\gamma\text{-Fe}_2\text{O}_3$  and  $\gamma\text{-Fe}_2\text{O}_3\text{@MCM-48}$  composite. A well ordered structure of MCM-48 was observed by XRD (Figure 4.1). At low diffraction angle in the  $2\theta$  range of 2.0-8.0 degree, X-ray diffractogram of the as-synthesized MCM-48 displays intensive diffraction peaks at  $2\theta$  of 2.6 and 3.1 degree, assigned to the (211) and (220) reflections, respectively. This information actually indicates the three-dimensional mesoporous structure with a Ia3d cubic space group [48]. In addition, all peaks can be indexed, corresponding to MCM-48 structure (JCPDS No.50-0511).

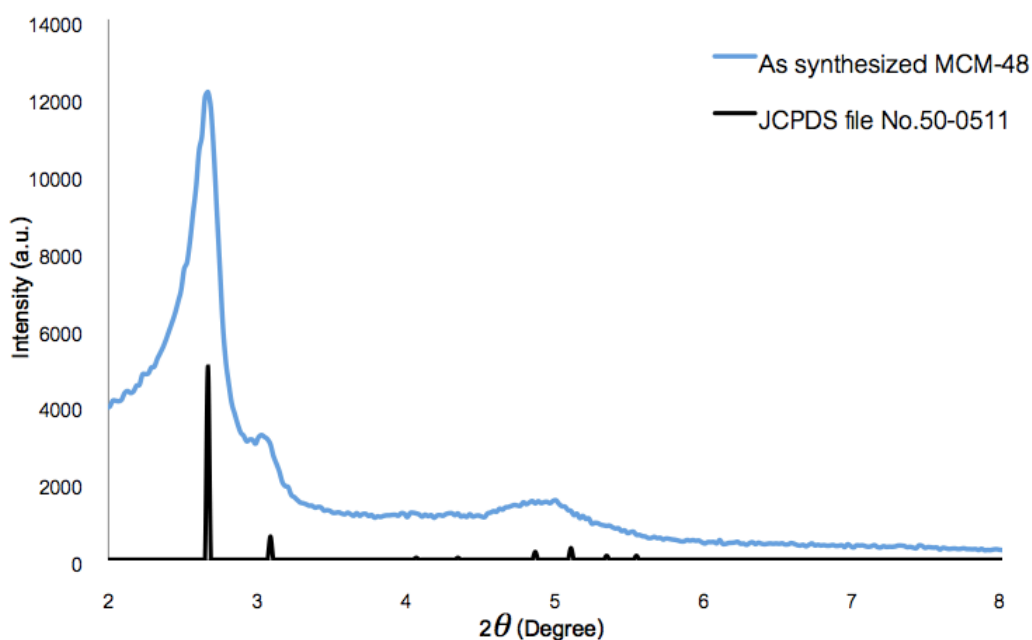
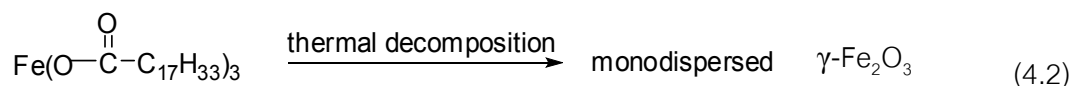
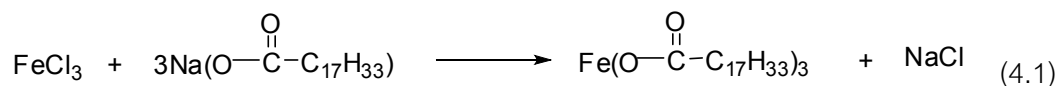


Figure 4.1 X-ray powder diffraction pattern of the as-synthesized MCM-48 compared to JCPDS file No.50-0511 of MCM-48.

Monodisperse  $\gamma$ -Fe<sub>2</sub>O<sub>3</sub> nanoparticles were synthesized using a two-step procedure according to Eq. (4.1) and (4.2).



The crystal structure of the as-synthesized  $\gamma$ -Fe<sub>2</sub>O<sub>3</sub> nanoparticles was confirmed by X-ray powder diffraction (Figure 4.2). In high angle region of the  $2\theta$  range of 20-70 degree, diffraction peaks at 30.3, 35.6, 43.3, 53.8, 57.3 and 62.9 degree corresponding to (220), (311), (400), (422), (511) and (440) reflections, respectively. These can be indexed and matched to JCPDS No.39-1346 of the  $\gamma$ -Fe<sub>2</sub>O<sub>3</sub> nanoparticles [63].

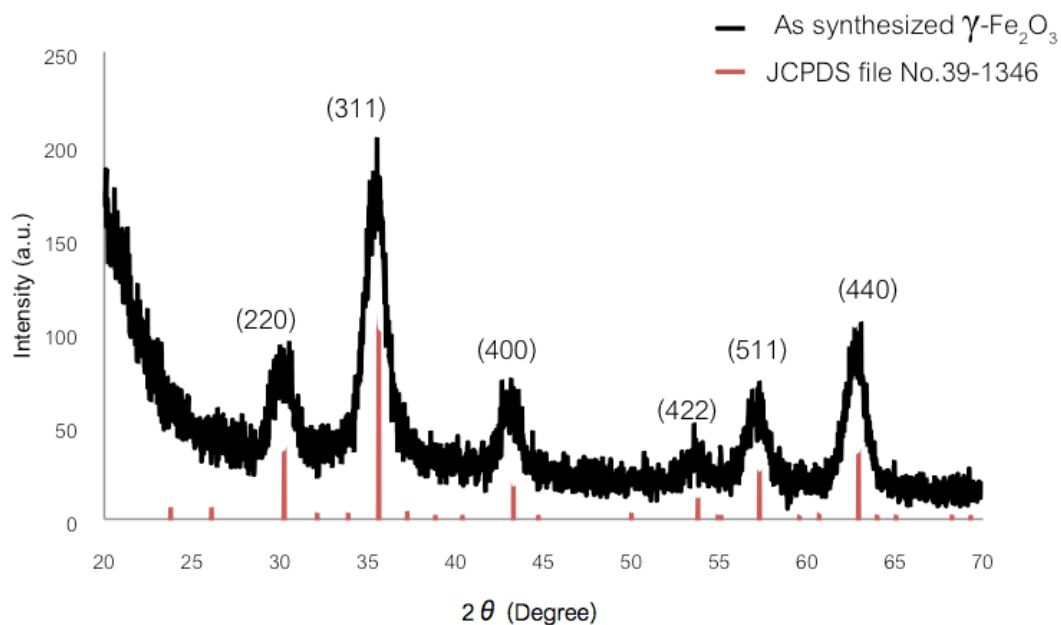
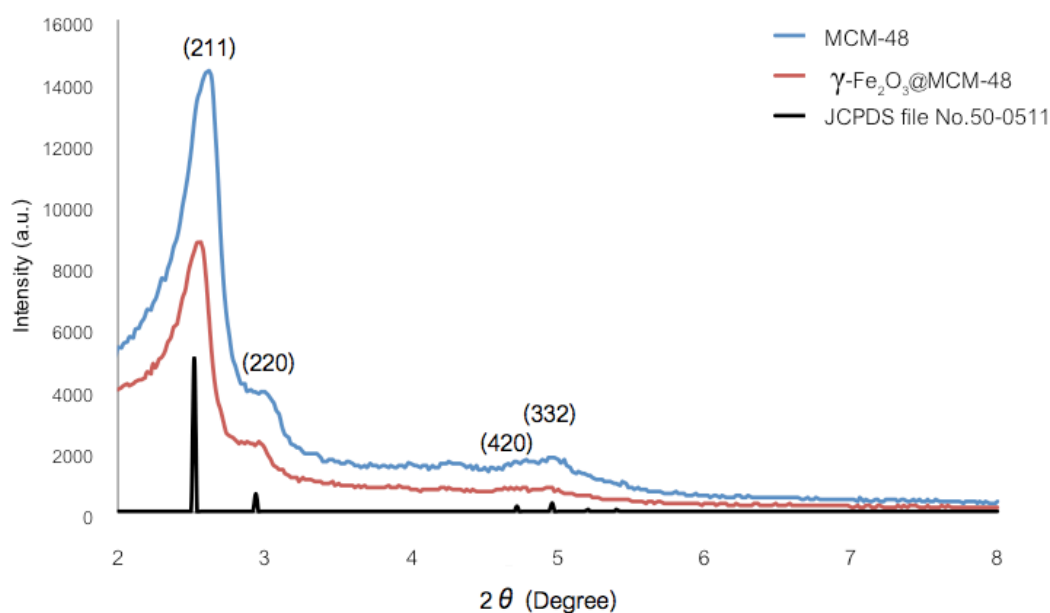


Figure 4.2 X-ray powder diffraction pattern of the as-synthesized  $\gamma$ -Fe<sub>2</sub>O<sub>3</sub> compared to JCPDS file No.39-1346 of  $\gamma$ -Fe<sub>2</sub>O<sub>3</sub>.

A composite of MCM-48 and  $\gamma\text{-Fe}_2\text{O}_3$  nanoparticles ( $\gamma\text{-Fe}_2\text{O}_3\text{@MCM-48}$ ) was synthesized and characterized by X-ray powder diffraction. The characteristic diffraction peaks of MCM-48 and  $\gamma\text{-Fe}_2\text{O}_3$  were also presented (Figure 4.3 and 4.4).

In low diffraction angle region ( $2\theta$  ranging from 2.0 to 8.0 degree) (Figure 4.3), the characteristic reflections of the MCM-48 structure ((211), (220), (420) and (332) reflections at  $2\theta$  degree of 2.6, 3.1, 4.9 and 5.1, respectively) were also observed in the diffractogram of  $\gamma\text{-Fe}_2\text{O}_3\text{@MCM-48}$  with lower intensity compared to raw MCM-48. These X-ray powder diffraction data indicate that cubic structure of MCM-48 was preserved after mixing with  $\gamma\text{-Fe}_2\text{O}_3$ .



**Figure 4.3** Low-angle X-ray powder diffraction patterns of MCM-48, 40%  $\gamma\text{-Fe}_2\text{O}_3\text{@MCM-48}$  and JCPDS file No.50-0511 of MCM-48.

In high diffraction angle region ( $2\theta$  ranging from 20 to 70 degree) (Figure 4.4), XRD pattern of  $\gamma\text{-Fe}_2\text{O}_3\text{@MCM-48}$  displays weak diffraction peaks at 30.3, 35.6, 43.3, 53.8, 57.3 and 62.9 that correspond to (220), (311), (400), (422), (511) and (440) reflections of  $\gamma\text{-Fe}_2\text{O}_3$  structure, respectively. It indicates that the structure of  $\gamma\text{-Fe}_2\text{O}_3$  in  $\gamma\text{-Fe}_2\text{O}_3\text{@MCM-48}$  composite was preserved. X-ray powder diffraction data confirm the coexistence of  $\gamma\text{-Fe}_2\text{O}_3$  phase in the MCM-48 structure. The composite also exhibited magnetic properties and responded to external magnetic field as shown in Figure 4.5.

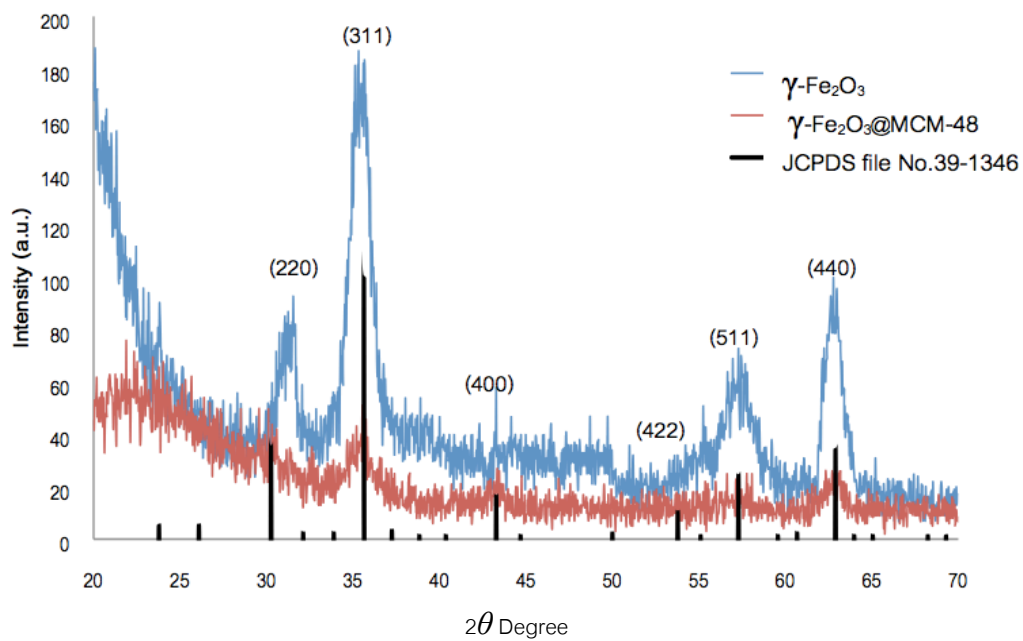


Figure 4.4 High-angle X-ray powder diffraction patterns of  $\gamma\text{-Fe}_2\text{O}_3$ , 40% $\gamma\text{-Fe}_2\text{O}_3\text{@MCM-48}$  and JCPDS file No.39-1346 of  $\gamma\text{-Fe}_2\text{O}_3$ .

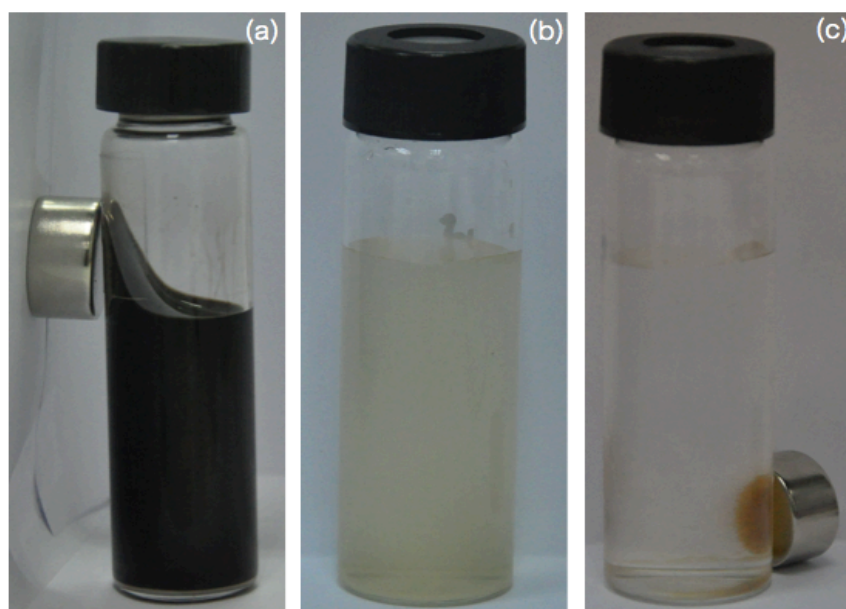


Figure 4.5 Magnetic properties exhibition of (a)  $\gamma\text{-Fe}_2\text{O}_3$ , (b) MP-40% $\text{Fe}_2\text{O}_3\text{@MCM-48}$  in solution before applying magnetic field and (c) MP-40% $\text{Fe}_2\text{O}_3\text{@MCM-48}$  in solution after applying magnetic field.



Furthermore, the influence of the amount of  $\gamma\text{-Fe}_2\text{O}_3$  and time in the synthesis of the adsorbents composite were studied in order to find the suitable condition that exhibited magnetic properties and had high surface area.

#### The effect of $\gamma\text{-Fe}_2\text{O}_3$ amount

Various quantities of  $\gamma\text{-Fe}_2\text{O}_3$  nanoparticles ranging from 40 to 80 percent of MCM-48 weight were used in the preparation of  $\gamma\text{-Fe}_2\text{O}_3\text{@MCM-48}$ . The content of the magnetic particles attached on the obtained composites was determined after extraction of the magnetic particles from composite (10 mg) using acid solution (100 mL). The concentrations of Fe in the extracted solutions were determined by FAAS. The theoretical and observed number of moles of  $\gamma\text{-Fe}_2\text{O}_3$  in  $\gamma\text{-Fe}_2\text{O}_3\text{@MCM-48}$  composite was calculated according to appendix and shown in Table 4.1.

**Table 4.1** Amount of  $\gamma\text{-Fe}_2\text{O}_3$  nanoparticles observed in  $\gamma\text{-Fe}_2\text{O}_3\text{@MCM-48}$  composites

Percent $\gamma\text{-Fe}_2\text{O}_3$ added	Theoretical amount of $\gamma\text{-Fe}_2\text{O}_3$ (mmol/g)	Observed amount of $\gamma\text{-Fe}_2\text{O}_3$ (mmol/g)
40%	1.79	0.191±0.004
50%	2.09	0.256±0.005
60%	2.35	0.301±0.009
70%	2.58	0.299±0.012
80%	2.78	0.300±0.003

According to the results in Table 4.1, when the starting amount of  $\gamma\text{-Fe}_2\text{O}_3$  nanoparticles was increased from 40 to 60 % (w/w) of MCM-48, the observed amount of  $\gamma\text{-Fe}_2\text{O}_3$  nanoparticles in  $\gamma\text{-Fe}_2\text{O}_3\text{@MCM-48}$  composites slightly increased and reached relatively constant value at 60% of starting amount of  $\gamma\text{-Fe}_2\text{O}_3$  nanoparticles, with maximum percent deposition of  $\gamma\text{-Fe}_2\text{O}_3$  nanoparticles on MCM-48 of 12.8 %. When the starting amount of  $\gamma\text{-Fe}_2\text{O}_3$  nanoparticles was higher than 60 % (w/w) of MCM-48, the percent deposition of  $\gamma\text{-Fe}_2\text{O}_3$  nanoparticles on MCM-48 slightly decreased. These results might be explained that  $\gamma\text{-Fe}_2\text{O}_3$  nanoparticles with particles size of 5 to 12 nm could fit only on the pores of compatible size of MCM-48 (which had pore size in a range of 3-10 nm). The unattached  $\gamma\text{-Fe}_2\text{O}_3$  nanoparticles were further washed off by hexane and  $\text{HNO}_3$ .

### The effect of contact time between MCM-48 and $\gamma\text{-Fe}_2\text{O}_3$

The synthesis of  $\gamma\text{-Fe}_2\text{O}_3\text{@MCM-48}$  was studied using contact time varied from 1 to 5 hours and 40% of starting amount of  $\gamma\text{-Fe}_2\text{O}_3$  nanoparticles were adopted. The content of magnetic nanoparticles in the obtained composites are determined and shown in Figure 4.6.

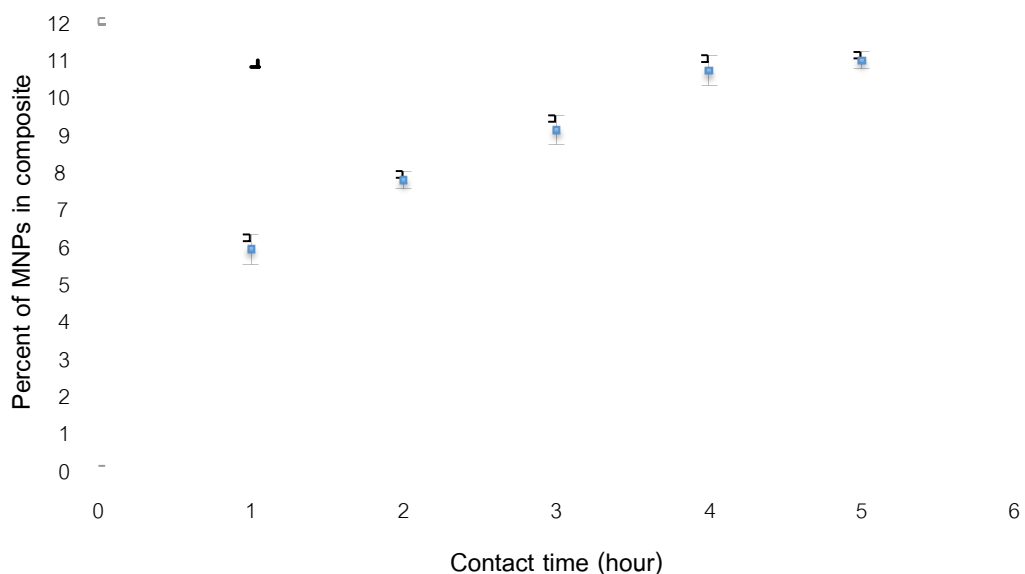


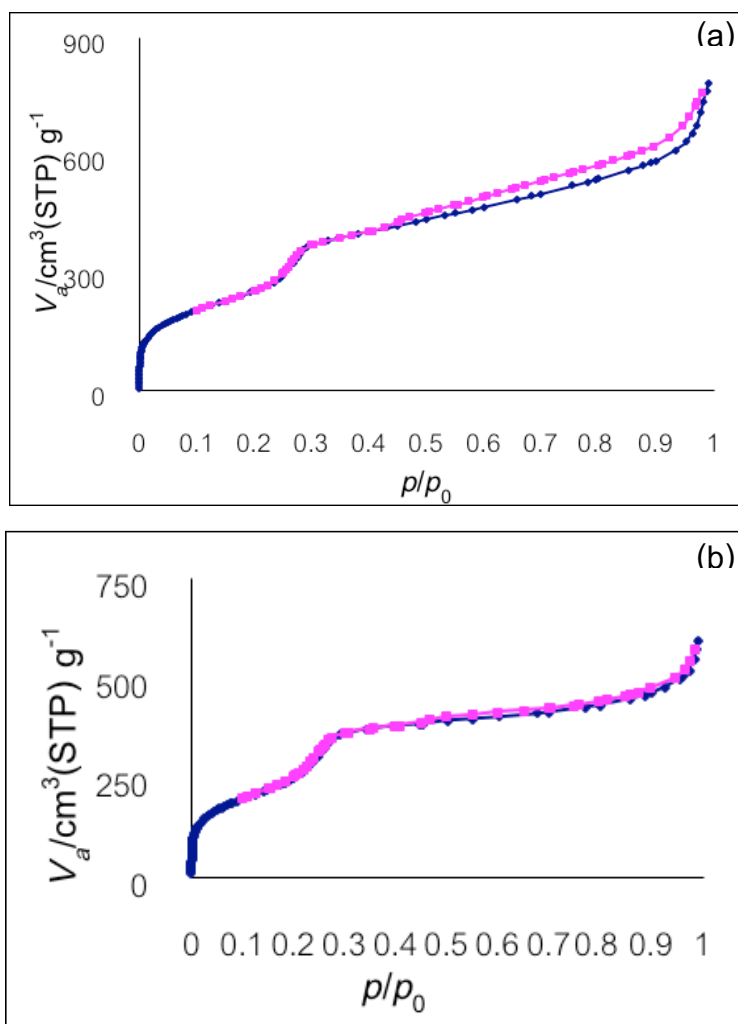
**Figure 4.6** Amount of  $\gamma\text{-Fe}_2\text{O}_3$  nanoparticles in  $\gamma\text{-Fe}_2\text{O}_3\text{@MCM-48}$  prepared by using different contact time between  $\gamma\text{-Fe}_2\text{O}_3$  and MCM-48.

According to the results in Figure 4.6, the percent deposition of  $\gamma\text{-Fe}_2\text{O}_3$  nanoparticles on MCM-48 slightly increased when the contact time increased, and reached relatively constant value at 4 hours of contact time. It is most likely because  $\gamma\text{-Fe}_2\text{O}_3$  nanoparticles could be throughout dispersed and deposited in most of the fittable pore on MCM-48 in 4 hours. Therefore, 4 hours of contact time were suitable to synthesize  $\gamma\text{-Fe}_2\text{O}_3\text{@MCM-48}$  in this research. Then the as-synthesized  $\gamma\text{-Fe}_2\text{O}_3\text{@MCM-48}$  composites were characterized and compared to the starting MCM-48.

## 4.1 Characterization

### 4.1.1 Characterization by surface area analyzer

Isotherms of nitrogen adsorption on MCM-48, and 40-70%  $\gamma$ -Fe<sub>2</sub>O<sub>3</sub>@MCM-48 (40% $\gamma$ -Fe<sub>2</sub>O<sub>3</sub>@MCM-48, 50% $\gamma$ -Fe<sub>2</sub>O<sub>3</sub>@MCM-48, 60% $\gamma$ -Fe<sub>2</sub>O<sub>3</sub>@MCM-48 and 70%  $\gamma$ -Fe<sub>2</sub>O<sub>3</sub>@MCM-48) were studied. Their surface area was calculated based on Brunauer Emmett Teller (BET) method. To obtain effective magnetic adsorbents, high surface area is required, along with magnetic properties. The higher surface area of the adsorbents, the higher adsorption efficiency would be obtained. The isotherms are shown in Figure 4.7.



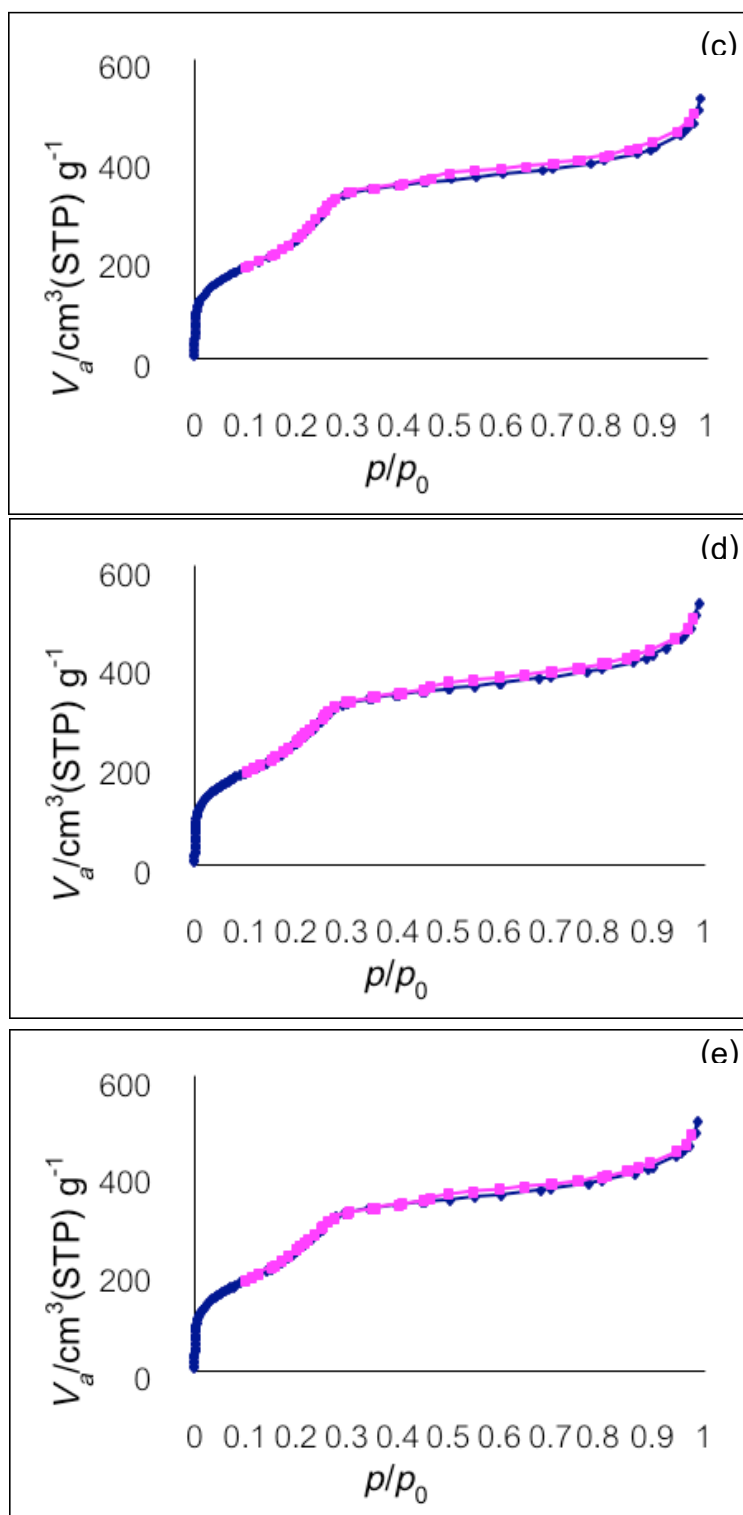


Figure 4.7 Isotherm of  $\text{N}_2$  adsorption by (a) MCM-48, (b) 40%  $\gamma\text{-Fe}_2\text{O}_3$ @MCM-48, (c) 50%  $\gamma\text{-Fe}_2\text{O}_3$ @MCM-48, (d) 60%  $\gamma\text{-Fe}_2\text{O}_3$ @MCM-48 and (e) 70%  $\gamma\text{-Fe}_2\text{O}_3$ @MCM-48.

The nitrogen adsorption isotherms of MCM-48 and  $\gamma\text{-Fe}_2\text{O}_3\text{@MCM-48}$  composites show defined step between  $P/P_0 = 0.1$  and  $0.3$ , indicating the filling into mesoporous structure. All of the sorption isotherms were type IV isotherm according to the IUPAC nomenclature [64], confirming that the as-synthesized MCM-48 and all of the composites were mesoporous materials. These sorption isotherms data were used to calculate the specific surface area by BET method ( $S_{\text{BET}}$ ) and average pore diameter as shown in Table 4.2.

**Table 4.2** Surface area and pore diameter of the materials

Materials	BET surface area ( $\text{m}^2/\text{g}$ )	Average pore diameter (nm)
MCM-48	$941 \pm 3$	$5.02 \pm 0.51$
40% $\gamma\text{-Fe}_2\text{O}_3\text{@MCM-48}$	$850 \pm 16$	$4.22 \pm 0.24$
50% $\gamma\text{-Fe}_2\text{O}_3\text{@MCM-48}$	$832 \pm 10$	$3.93 \pm 0.13$
60% $\gamma\text{-Fe}_2\text{O}_3\text{@MCM-48}$	$819 \pm 11$	$4.02 \pm 0.11$
70% $\gamma\text{-Fe}_2\text{O}_3\text{@MCM-48}$	$800 \pm 17$	$3.84 \pm 0.35$
40% MP- $\text{Fe}_2\text{O}_3\text{@MCM-48}$	678	3.89

BET surface area and average pore diameter of the as-synthesized MCM-48 were  $941.67 \text{ m}^2/\text{g}$  and  $5.02 \text{ nm}$ , respectively. When  $\gamma\text{-Fe}_2\text{O}_3\text{@MCM-48}$  was prepared by using 40-70% w/w of  $\gamma\text{-Fe}_2\text{O}_3$ , BET surface area of the obtained composites decreased, most likely due to the presence of  $\gamma\text{-Fe}_2\text{O}_3$  on the surface which partially blocked the channels of MCM-48. The saturated pressure (Y axis in Figure 4.7) also decreased. The higher content of  $\gamma\text{-Fe}_2\text{O}_3$  deposited, the lower porosity of  $\gamma\text{-Fe}_2\text{O}_3\text{@MCM-48}$  composites was observed. These results indicate that  $\gamma\text{-Fe}_2\text{O}_3$  nanoparticles were incorporated onto MCM-48 and however the pore system of MCM-48 framework was still accessible.

According to the content of  $\gamma\text{-Fe}_2\text{O}_3$  nanoparticles in all of the obtained  $\gamma\text{-Fe}_2\text{O}_3\text{@MCM-48}$  composites and their surface area, using the amount of  $\gamma\text{-Fe}_2\text{O}_3$  nanoparticles higher than 40% of MCM-48 weight was not beneficial and it was a waste of material. Moreover, BET surface area of  $\gamma\text{-Fe}_2\text{O}_3\text{@MCM-48}$  prepared by using 40% of  $\gamma\text{-Fe}_2\text{O}_3$  nanoparticles was higher than that of the other composites. This might lead to higher efficiency in mercury adsorption. Therefore,  $\gamma\text{-Fe}_2\text{O}_3$  nanoparticles amount of 40% of MCM-48 weight was chosen in the next synthesis.

When 40%  $\gamma\text{-Fe}_2\text{O}_3\text{@MCM-48}$  composites were functionalized with (3-mercaptopropyl)trimethoxysilane (MP) to produce  $\text{MP-Fe}_2\text{O}_3\text{@MCM-48}$ , BET surface area and average pore diameter of  $\text{MP-Fe}_2\text{O}_3\text{@MCM-48}$  decreased to  $677.58\text{ m}^2/\text{g}$  and  $3.89\text{ nm}$ , respectively, as shown in Table 4.2. It is because the functionalized molecules occupied the surface and the pore of the adsorbent.

## 4.2 Characterization of $\gamma\text{-Fe}_2\text{O}_3\text{@MCM-48}$ morphology by SEM and TEM

### 4.2.1 Morphology by scanning electron microscopy (SEM)

Morphology of  $\gamma\text{-Fe}_2\text{O}_3\text{@MCM-48}$  was illustrated by SEM as shown in Figure 4.8.

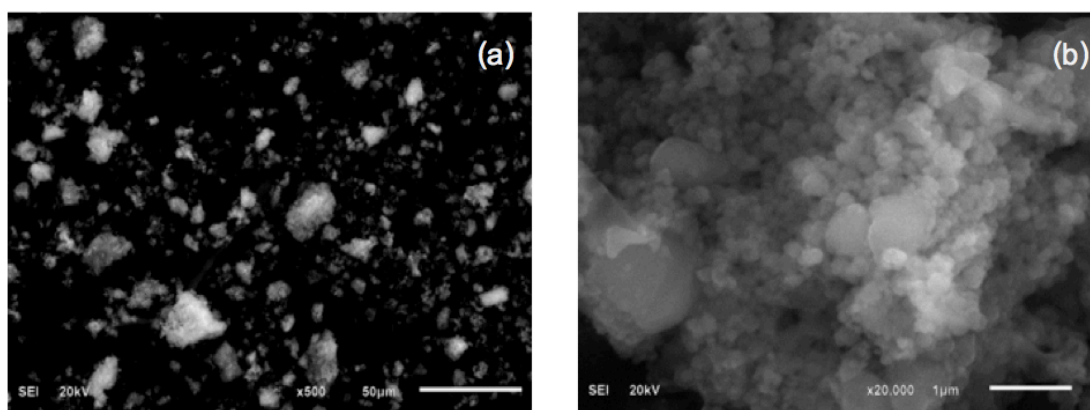


Figure 4.8 SEM images of 40%  $\gamma\text{-Fe}_2\text{O}_3\text{@MCM-48}$  composites with (a) low and (b) high magnifications.

The SEM images of  $\gamma\text{-Fe}_2\text{O}_3\text{@MCM-48}$  reveal the spherical particles and some aggregation of  $\gamma\text{-Fe}_2\text{O}_3\text{@MCM-48}$  particles. The particles size of  $\gamma\text{-Fe}_2\text{O}_3\text{@MCM-48}$  was  $240\pm 40\text{ nm}$  in diameter.

### 4.2.2 Morphology by transmission electron microscopy (TEM)

Ordered pore structure of the as-synthesized MCM-48 was illustrated by TEM. Figure 4.9(a) shows that the particles of MCM-48 are spherical with highly ordered pore structure. TEM images also show that the pore structures of MCM-48 are cubic (Figure 4.9(b)).

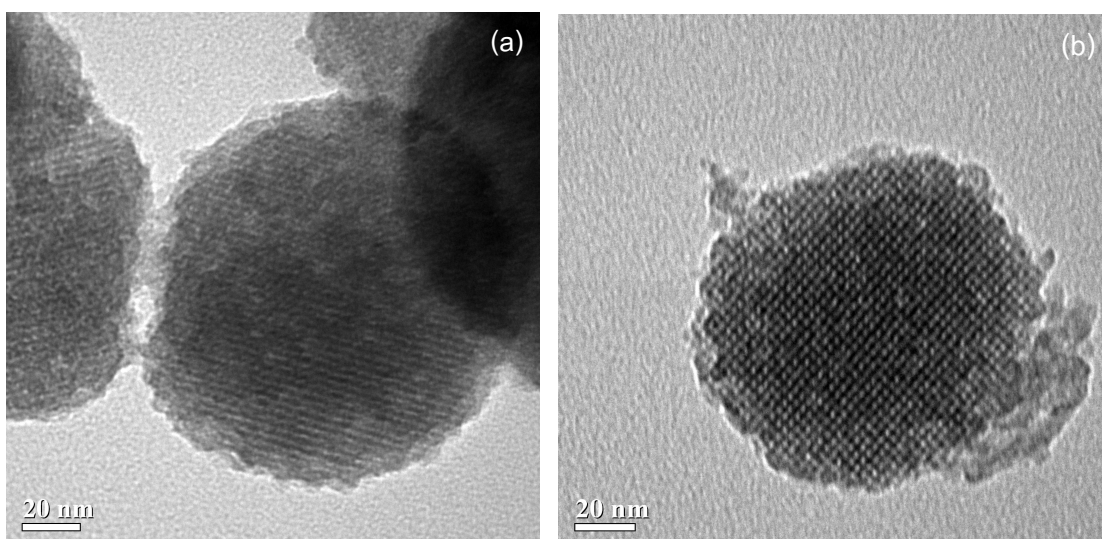


Figure 4.9 TEM images of the as-synthesized MCM-48.

TEM images of  $\gamma\text{-Fe}_2\text{O}_3$  particles dispersed in hexane (Figure 4.10) show highly monodisperse  $\gamma\text{-Fe}_2\text{O}_3$  particles of uniform spherical shape and particle size of 5 to 12 nm. Each particle was well separated from its neighbors most likely due to the presence of residual oleic acid that was absorbed on particles via interaction with iron atoms [65] as shown in Scheme 4.1.

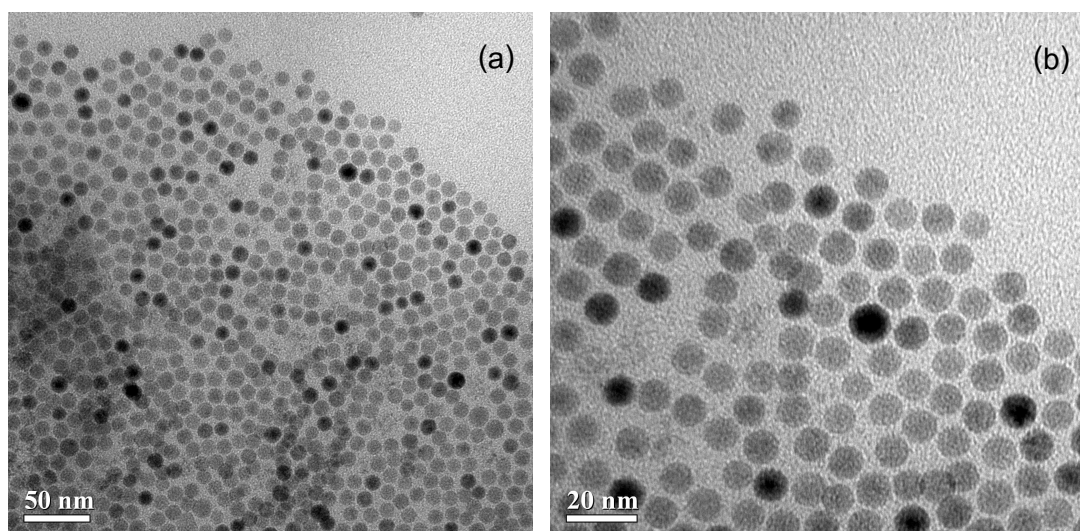
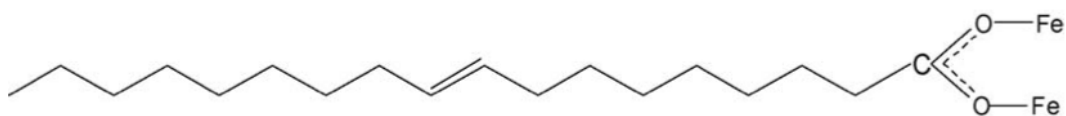
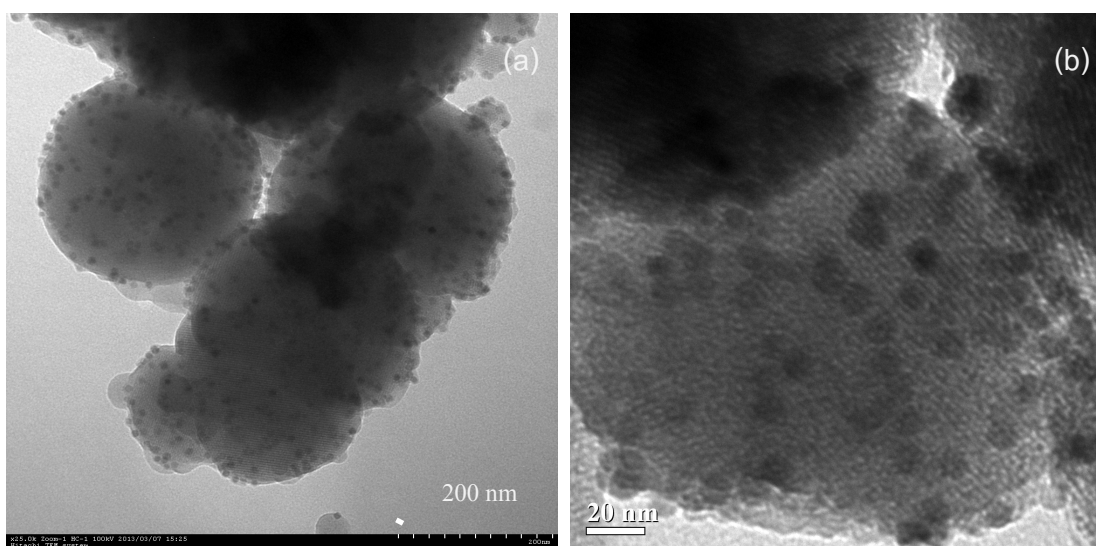


Figure 4.10 TEM images of the as-synthesized  $\gamma\text{-Fe}_2\text{O}_3$  with (a) low and (b) high magnifications.



**Scheme 4.1** Interaction between  $\text{COO}^-$  group of oleic acid and iron atoms [65].

TEM images of  $\gamma\text{-Fe}_2\text{O}_3\text{@MCM-48}$  composites are shown in Figure 4.11. It reveals some aggregation of  $\gamma\text{-Fe}_2\text{O}_3\text{@MCM-48}$  particles with  $\gamma\text{-Fe}_2\text{O}_3$  nanoparticles deposited mostly on outer surface of MCM-48. It can be seen that  $\gamma\text{-Fe}_2\text{O}_3$  nanoparticles can distribute throughout MCM-48. It seems that a good dispersion of  $\gamma\text{-Fe}_2\text{O}_3$  nanoparticles in hexane led to a good distribution of the nanoparticles throughout MCM-48 surface. TEM images also confirm the deposition and coexistence of  $\gamma\text{-Fe}_2\text{O}_3$  phase in MCM-48 structure.



**Figure 4.11** TEM images of the 40%  $\gamma\text{-Fe}_2\text{O}_3\text{@MCM-48}$  composites with (a) low and (b) high magnifications.

#### 4.3 Surface modification with 3-mercaptopropyl trimethoxysilane

3-mercaptopropyl trimethoxysilane was used to modify onto the surface of  $\gamma\text{-Fe}_2\text{O}_3\text{@MCM-48}$  using grafting method via the condensation of the hydroxyl group ( $-\text{OH}$ ) on the surface with ethoxy group ( $-\text{OCH}_2\text{CH}_3$ ) of the 3-mercaptopropyl trimethoxysilane. The modified  $\gamma\text{-Fe}_2\text{O}_3\text{@MCM-48}$  ( $\text{MP-Fe}_2\text{O}_3\text{@MCM-48}$ ) was characterized by Fourier



transforms infrared spectrometry (FT-IR) to investigate the presence of specific organic functional groups and surface chemical compositions of the materials. FT-IR spectra of MCM-48,  $\gamma\text{-Fe}_2\text{O}_3\text{@MCM-48}$  and  $\text{MP-Fe}_2\text{O}_3\text{@MCM-48}$  were recorded using potassium bromide (KBr) technique.

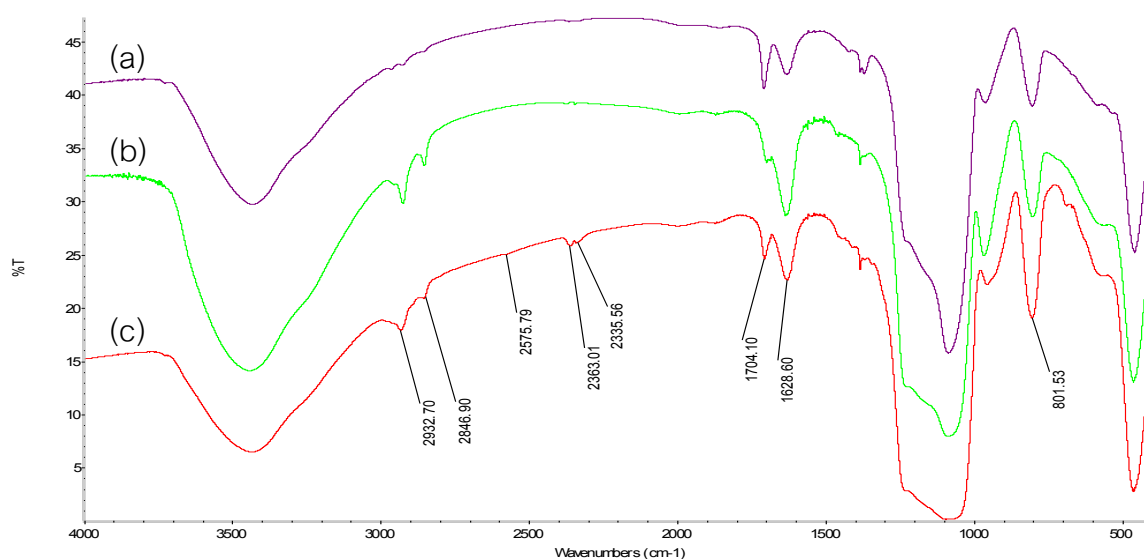


Figure 4.12 FT-IR spectra of (a) MCM-48, (b)  $\gamma\text{-Fe}_2\text{O}_3\text{@MCM-48}$  and (c)  $\text{MP-Fe}_2\text{O}_3\text{@MCM-48}$ .

Figure 4.12 (a) shows the IR patterns of MCM-48 between 4000 and 400  $\text{cm}^{-1}$ . The main features of the MCM-48 spectrum are a large broad band between 3400 and 3200  $\text{cm}^{-1}$  which is attributed to O-H bond stretching [66] of the surface silanol group. The deformational vibrations band of adsorbed water molecules of MCM-48 was detected at 1632  $\text{cm}^{-1}$  [67]. Si-O-Si stretching appeared at 1233 and 1079  $\text{cm}^{-1}$ . Si-O stretching was detected at 962 and 804  $\text{cm}^{-1}$  [68].

In Figure 4.12 (b), the IR spectrum of  $\gamma\text{-Fe}_2\text{O}_3\text{@MCM-48}$  presents characteristic band of silanol O-H stretching at 3447  $\text{cm}^{-1}$ . Si-O-Si stretching at 1233 and 1069  $\text{cm}^{-1}$  and Si-O stretching at 962 and 804  $\text{cm}^{-1}$  were also observed. The symmetric aliphatic C-H stretching and asymmetric aliphatic C-H stretching were detected at 2850  $\text{cm}^{-1}$  and 2922  $\text{cm}^{-1}$ , respectively. The presence of aliphatic hydrocarbon in the material was likely due to the presence of residual oleate in monodisperse  $\gamma\text{-Fe}_2\text{O}_3$  that absorbed onto

MCM-48 [65]. And the intensity of band at  $1628\text{ cm}^{-1}$  changed, also due to the symmetric ( $\text{COO}^-$ ) stretch of the residual oleate.

FT-IR spectrum of  $\text{MP-Fe}_2\text{O}_3@\text{MCM-48}$  is shown in Figure 4.12 (c). Characteristic band for silanol group O-H stretching at  $3447\text{ cm}^{-1}$ , Si-O-Si stretching at  $1233$  and  $1069\text{ cm}^{-1}$  and Si-O stretching at  $962$  and  $804\text{ cm}^{-1}$  were also observed. These bands are attributed to functional groups of MCM-48. The C-H stretching at  $2850\text{ cm}^{-1}$   $2922\text{ cm}^{-1}$  were still present in IR spectra of  $\text{MP-Fe}_2\text{O}_3@\text{MCM-48}$  and it could be attributed to the CH stretching in the molecule of oleate and also mercaptopropyl trimethoxysilane. The signal of S-H stretching of the attached MP group at  $2575\text{ cm}^{-1}$  [69] was absent due to its weak intensity, while the peaks at  $2363$  and  $2335\text{ cm}^{-1}$  which are also signal of S-H stretching [70] were observed. The results of FT-IR could confirm that MP was actually modified onto the adsorbent.

## Part II Adsorption study

### 4.4 Adsorption study

#### 4.4.1 Preliminary study

3-(mercaptopropyl)-trimethoxysilane modified 40%  $\gamma\text{-Fe}_2\text{O}_3@\text{MCM-48}$ , 50%  $\gamma\text{-Fe}_2\text{O}_3@\text{MCM-48}$ , 60%  $\gamma\text{-Fe}_2\text{O}_3@\text{MCM-48}$  and 70%  $\gamma\text{-Fe}_2\text{O}_3@\text{MCM-48}$  were used to remove Hg(II) ions in 50 mL solution. The initial concentration of Hg(II) solution and the pH was 10 mg/L and 5, respectively and 10 mg of each adsorbent was used. The percentage removal of Hg(II) is shown in Table 4.3.

**Table 4.3** Adsorption efficiency of  $\text{MP-Fe}_2\text{O}_3@\text{MCM-48}$  composites prepared using different amount of  $\gamma\text{-Fe}_2\text{O}_3$

Materials	Removal efficiency (%)	Amount of Hg(II) adsorbed (mg/g)
40% $\text{Fe}_2\text{O}_3@\text{MCM-48}$	0.33	0.16
MP-40% $\text{Fe}_2\text{O}_3@\text{MCM-48}$	99.96	48.48
MP-50% $\text{Fe}_2\text{O}_3@\text{MCM-48}$	99.95	48.48
MP-60% $\text{Fe}_2\text{O}_3@\text{MCM-48}$	99.90	48.48
MP-70% $\text{Fe}_2\text{O}_3@\text{MCM-48}$	99.88	48.47

The results from experiments suggest that the unmodified  $\gamma$ -Fe<sub>2</sub>O<sub>3</sub>@MCM-48 composite (40%Fe<sub>2</sub>O<sub>3</sub>@MCM-48) could only slightly adsorb Hg(II) in solution due to electrostatic interaction between silyanol groups and Hg(II) ions. On the other hand, MP-Fe<sub>2</sub>O<sub>3</sub>@MCM-48 composites can be used as effective adsorbents for Hg(II) removal from aqueous solution because it contained donor atoms which can coordinate with Hg(II). Moreover, MP-Fe<sub>2</sub>O<sub>3</sub>@MCM-48 prepared by using 40 to 70 % w/w of  $\gamma$ -Fe<sub>2</sub>O<sub>3</sub> could remove Hg(II) ions from aqueous solution with high adsorption efficiency. Considering the content of  $\gamma$ -Fe<sub>2</sub>O<sub>3</sub> nanoparticles in all of the obtained  $\gamma$ -Fe<sub>2</sub>O<sub>3</sub>@MCM-48 composites (Table 4.1), BET surface area data (Table 4.2) and the adsorption efficiency of the functionalized composites, the results indicate that the change in the starting amount of  $\gamma$ -Fe<sub>2</sub>O<sub>3</sub> nanoparticles from 40 % to 80 % did not result in an improvement in magnetic particles content, surface area and the adsorption efficiency. In addition, all composites showed response to external magnetic field. Consequently, the composites prepared by using  $\gamma$ -Fe<sub>2</sub>O<sub>3</sub> nanoparticles at 40 % of MCM-48 weight were chosen for Hg(II) adsorption due to the use of least quantities of  $\gamma$ -Fe<sub>2</sub>O<sub>3</sub> while magnetic properties for magnetic separation was still achievable.

In the adsorption study, the volume of Hg(II) solution was reduced from 50 mL to 25 mL, in order to reduce the volume of mercury waste generated from the experiment and MP-Fe<sub>2</sub>O<sub>3</sub>@MCM-48 adsorbent weight was also reduced to 5 mg to keep the same solid/liquid ratio.

To study the adsorption behavior, the effect of pH and adsorption time on the adsorption of Hg(II) onto MP-Fe<sub>2</sub>O<sub>3</sub>@MCM-48 was studied. The efficiency in metal removal from solution by the adsorbents is presented as percentage removal calculated by using the following Equation;

$$\text{Removal (\%)} = \frac{C_i - C_f}{C_i} \times 100 \quad (4.2)$$

where  $C_i$  and  $C_f$  are the initial and final concentration of Hg(II) in solution (mg/L), respectively.

#### 4.4.2 Effect of pH of Hg(II) ions solutions

The initial pH of mercury solution was varied in a range of 1 to 6. The effect of pH on the efficiency of mercury adsorption on MP-Fe<sub>2</sub>O<sub>3</sub>@MCM-48 is shown in Figure 4.13.

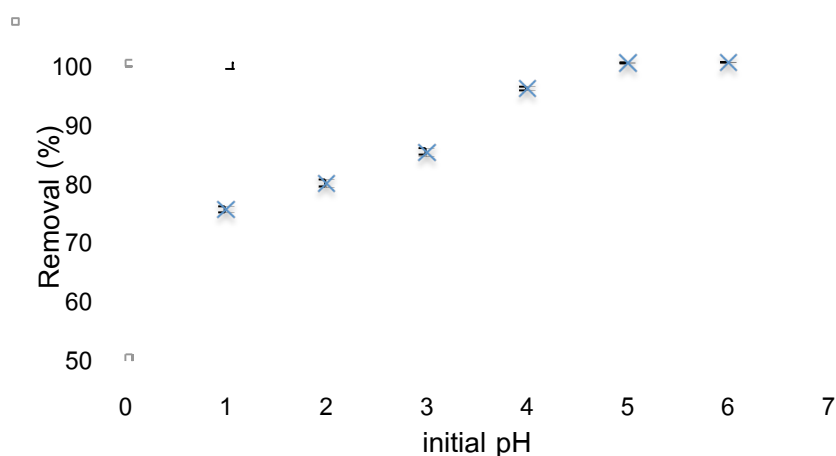


**Figure 4.13** Effect of pH on Hg(II) adsorption on MP-Fe<sub>2</sub>O<sub>3</sub>@MCM-48; initial concentration 40 mg/L; adsorption time 60 minutes.

It was found that, MP-Fe<sub>2</sub>O<sub>3</sub>@MCM-48 could remove Hg(II) ions with high removal efficiency (75.3 %), even in strong acid solution. When the initial pH of solution increased, the efficiency in mercury removal also increased and reached a constant value at the initial pH around 5. The results could be explained by the difference in affinity of electron donor atoms (sulfur atoms) of thiol groups towards different species of Hg(II) in solution with different pH values that causes the change in adsorbed amount of Hg(II) and hence change in percent mercury removal as shown in Hg(II) speciation diagram Figure 4.14.

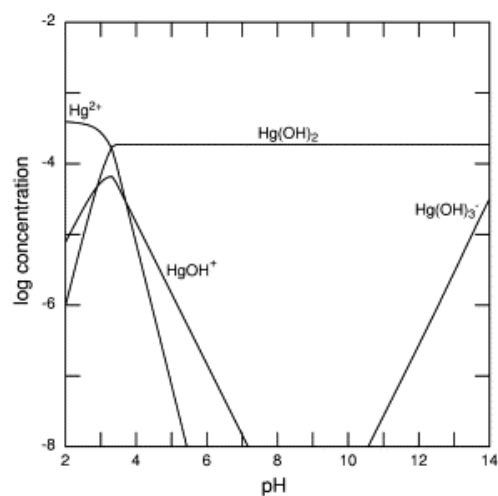
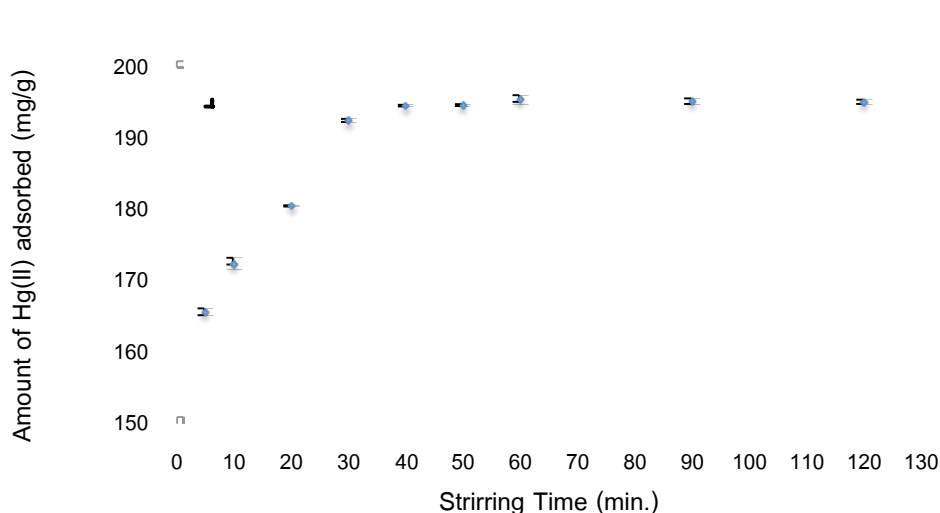


Figure 4.14 Aqueous speciation diagram of Hg(II) at different solution pH [71].

$\text{Hg}^{2+}$  cations and  $\text{Hg(OH)}^+$  species appeared in solution with pH value less than 4. The coordination of  $\text{Hg}^{2+}$  and  $\text{Hg(OH)}^+$  with  $-\text{SH}$  groups may lead to the formation of positively charged complexes on surface, which would prevent free mercury cations to approach the other available function groups on surface via electrostatic repulsion between the positively charged surface and metal cations, resulting in low adsorption efficiency. In solution with pH value higher than 4, the major species of Hg(II) ions are the neutral  $\text{Hg(OH)}_2$  species. Based on hard-soft acid base theory, the coordination of  $\text{Hg(OH)}_2$  with the  $-\text{SH}$  groups (soft base) would be highly favorable because neutral molecule are softer acid than metal cations. Thus, the percentage of Hg(II) ions removal from solutions with pH values higher than 4 were greater than that observed in solutions with pH values lower than 4 and the percent removal of Hg(II) increased and reached a constant value at pH around 5. In conclusion, the suitable pH for Hg(II) ions adsorption was initial pH of 5 and higher.

#### 4.4.3 Effect of adsorption time

The time to reach the equilibrium of Hg(II) adsorption on  $\text{MP-Fe}_2\text{O}_3@\text{MCM-48}$  under the studied experimental condition was studied at pH 6 by varying the adsorption time in time period of 5 to 120 minutes. The amount of Hg(II) adsorbed by  $\text{MP-Fe}_2\text{O}_3@\text{MCM-48}$  as function of time is shown in Figure 4.15.



**Figure 4.15** Effect of adsorption time on Hg(II) adsorption on MP-Fe<sub>2</sub>O<sub>3</sub>@MCM-48; initial concentration 40 mg/L; pH 6.

The results show that within only 5 minutes, MP-Fe<sub>2</sub>O<sub>3</sub>@MCM-48 could remove Hg(II) ions with high adsorption capacity (164.7 mg/g), indicating that MP-Fe<sub>2</sub>O<sub>3</sub>@MCM-48 has the fast kinetics of adsorption. Although, the amount of Hg(II) adsorbed increased with the increasing of contact time and reached the equilibrium after 40 minutes. But in further experiments, especially in adsorption isotherm study, higher concentration of mercury solution would be used and then the equilibrium would be reached in longer time. Therefore, the adsorption time of 60 minutes was chosen.

#### 4.4.4 Adsorption isotherms

The adsorption behavior of Hg(II) on the MP-Fe<sub>2</sub>O<sub>3</sub>@MCM-48 at equilibrium can be explained by the results obtained from the study of adsorption isotherms. The experiments were performed by using fixed amount of MP-Fe<sub>2</sub>O<sub>3</sub>@MCM-48 (5 mg) and fixed volume of metal solution (25 mL) containing various concentration of Hg(II) solution (10-400 mg/L) with pH value of 6; adsorption time 60 minutes at 25 °C. The equilibrium adsorption data obtained were further fitted to different isotherm models.

Langmuir and Freundlich relations are the two models adopted in this study. Langmuir isotherm is used based on the assumption that the adsorption occurs as monolayer coverage of analytes on homogeneous surface with limited number of active sites. Only one target metal ion would be adsorbed on each site via chemisorption. On the other hand, Freundlich isotherm is the model that was proposed based on

adsorption of analytes on surface bearing different active sites with different adsorption energy. Metal ions could be adsorbed on these active sites on adsorbent surface as multilayer coverage.

Figure 4.16 displays the amount of Hg(II) adsorbed by MP-Fe<sub>2</sub>O<sub>3</sub>@MCM-48 adsorbent after increasing the initial Hg(II) concentration. The amount of Hg(II) adsorbed on adsorbent increased rapidly at low initial concentration and reached a constant value around 200 mgHg/g sorbent when initial concentration of Hg(II) solution was 50 mg/L and higher, indicating the saturation of Hg(II) on active sites on adsorbent surface.

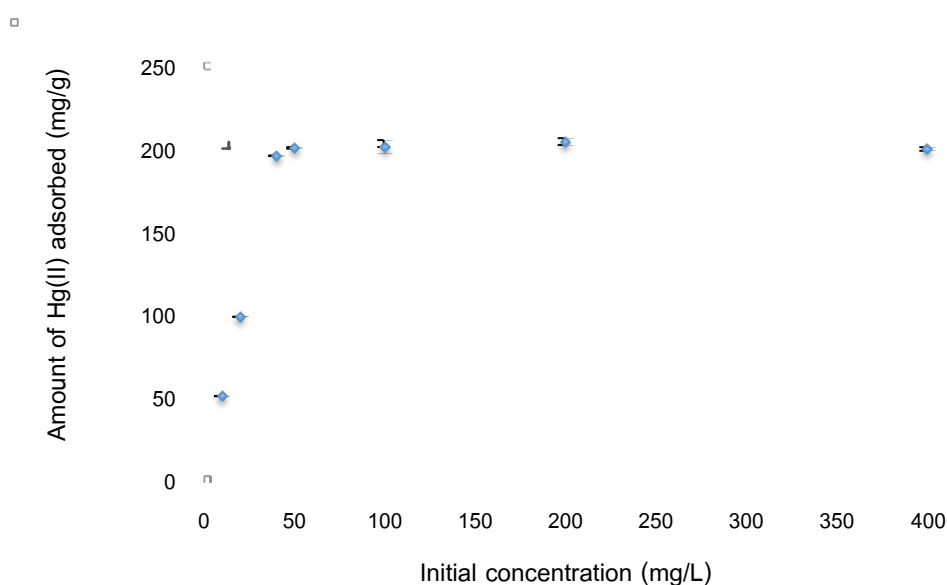


**Figure 4.16** Adsorption isotherm of Hg(II) adsorption on MP-Fe<sub>2</sub>O<sub>3</sub>@MCM-48; pH 6; adsorption time 60 minutes.

The experimental data of Hg(II) adsorption were used for linear plotting according to linear form of Langmuir and Freundlich model equations as shown in Eq. 4.3 and 4.4.

The Langmuir equation can be written in linear form as given in Eq. 4.3 where  $q$  and  $C_e$  are amount of Hg(II) adsorbed at equilibrium (mg/g) and equilibrium concentration of Hg(II) in bulk solution (mg/L), respectively.

$$\frac{C_e}{q} = \frac{1}{q_m b} + \frac{C_e}{q_m} \quad (4.3)$$

The maximum adsorption capacity ( $q_m$ ) and Langmuir constant ( $b$ ) that is related to the energy of adsorption, can be calculated from slope and y-axis interception of the linear equation of the plot between  $C_e/q_e$  versus  $C_e$  as shown in Figure 4.17.

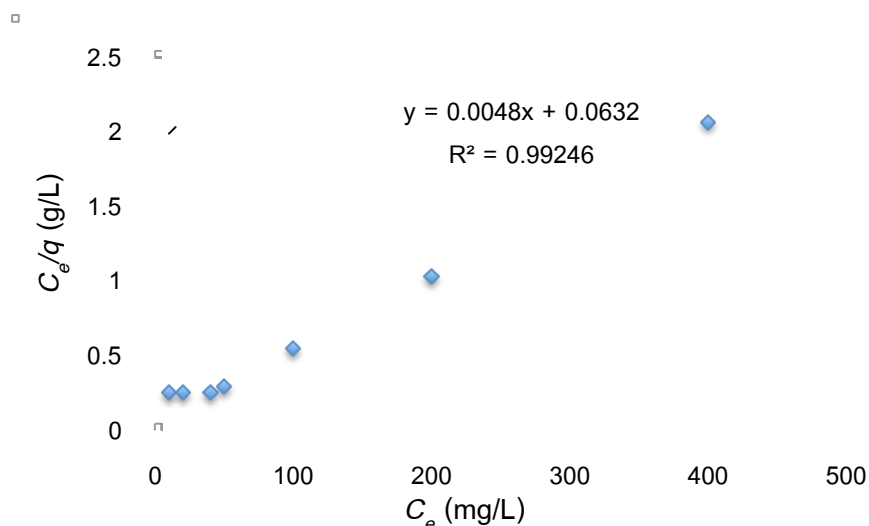


**Figure 4.17** Linear Langmuir plot of Hg(II) adsorption on MP-Fe<sub>2</sub>O<sub>3</sub>@MCM-48.

Furthermore, linear form of Freundlich equation is presented by the following equation, where  $K_f$  is a constant related to adsorption capacity of the adsorbent and  $n$  is Freundlich constant indicating the adsorption intensity.  $q_e$  and  $C_e$  are the amount of Hg(II) adsorbed (mg/g) at equilibrium and concentration at equilibrium (mg/L), respectively.

$$\ln q_e = \ln K_f + \frac{1}{n} \ln C_e \quad (4.4)$$

The equilibrium adsorption data fitted to linear form of Freundlich equation by plotting in  $q_e$  versus in  $C_e$  is presented in Figure 4.18.



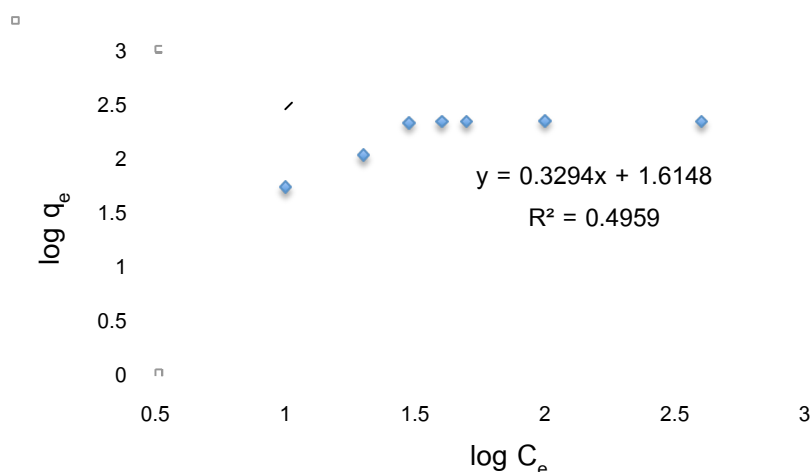


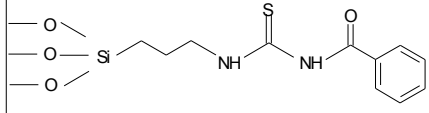
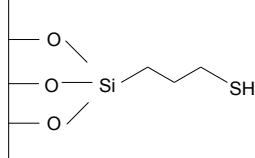
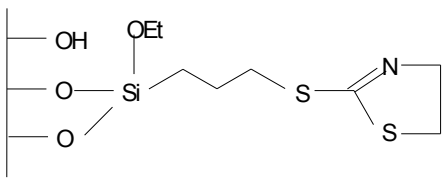
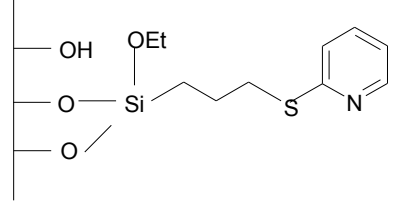
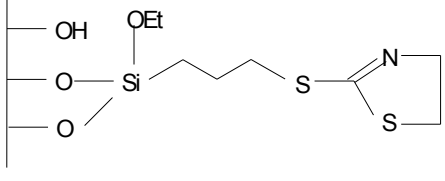
Figure 4.18 Linear Freundlich plot of Hg(II) adsorption on MP-Fe<sub>2</sub>O<sub>3</sub>@MCM-48.

In Figure 4.17 and 4.18, the obtained equation and correlation coefficient ( $R^2$ ) of linear line fit are shown. The experimental data of Hg(II) adsorption fit to Langmuir model ( $R^2 > 0.99$ ) better than Freundlich model, revealing that the behavior of Hg(II) adsorption on the MP-Fe<sub>2</sub>O<sub>3</sub>@MCM-48 adsorbent follows the assumption of Langmuir model. Langmuir constant ( $b$ ) calculated from the linear equation obtained was  $1.52 \times 10^4$  L/mol. The high  $b$  values relate to high adsorption energy of the adsorption that occurs via chemisorptions. In this study, it indicates that the sorption mechanism of Hg(II) ions on MP-Fe<sub>2</sub>O<sub>3</sub>@MCM-48 adsorbent occurred through the coordination of metals ions with donor sites of ligand (sulfur atom). The maximum adsorption capacity ( $q_m$ )<sub>cal</sub> of Hg(II) calculated from equation was 208.33 mg/g, which is in agreement with the maximum adsorption capacity observed in the experiment ( $q_m$ )<sub>exp</sub> (198.95-201.97 mg/g). It confirms that the experimental data were well fit to Langmuir isotherm.

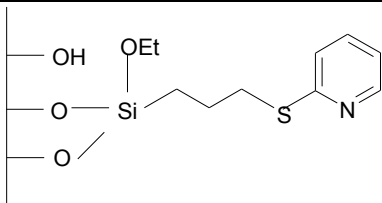
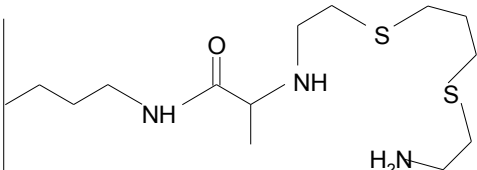
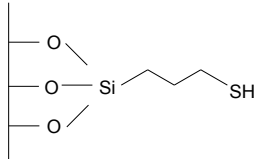
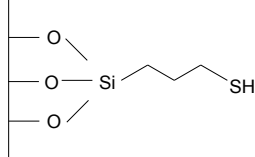
Table 4.4 The maximum adsorption capacity of the MP-Fe<sub>2</sub>O<sub>3</sub>@MCM-48 compared to other modified mesoporous silica for Hg(II) ions adsorption

Adsorbent	Modified surfaces	Adsorption capacity (mmol/g)	Reference
MCM-41	<p>Benzoylthiourea</p>	5.00	[47]

**Table 4.4** The maximum adsorption capacity of the MP-Fe<sub>2</sub>O<sub>3</sub>@MCM-48 compared to other modified mesoporous silica for Hg(II) ions adsorption (continued)

Adsorbent	Modified surfaces	Adsorption capacity (mmol/g)	Reference
MCM-48	 <p>Benzoylthiourea</p>	1.55	[48]
SBA-15	 <p>3-mercaptopropyltrimethoxysilane</p>	0.40	[49]
SBA-15	 <p>2-mercaptothiazoline</p>	1.10	[50]
SBA-15	 <p>2-mercaptopyridine</p>	0.16	[51]
MCM-41	 <p>2-mercaptothiazoline</p>	0.70	[50]

**Table 4.4** The maximum adsorption capacity of the MP-Fe<sub>2</sub>O<sub>3</sub>@MCM-48 compared to other modified mesoporous silica for Hg(II) ions adsorption (continued)

Adsorbent	Ligand	Adsorption capacity (mmol/g)	Reference
MCM-41	 <p>2-mercaptopyridine</p>	0.12	[51]
MCM-41	 <p>2-(3-(2-aminoethylthio)propylthio)ethanamine</p>	0.79	[52]
MCM-48	 <p>3-mercaptopropyltrimethoxysilane</p>	2.20	[12]
$\gamma$ -Fe <sub>2</sub> O <sub>3</sub> @MCM-48	 <p>3-mercaptopropyltrimethoxysilane</p>	1.04	This work

When compare the adsorption capacity of MP-Fe<sub>2</sub>O<sub>3</sub>@MCM-48 to other modified mesoporous silica reported by other authors (Table 4.4), the adsorbent prepared in this work shows a good capacity for Hg(II) adsorption. Despite the adsorbent prepared in

this work ( $\gamma$ -Fe<sub>2</sub>O<sub>3</sub>@MCM-48) shows less adsorption capacity than that of MCM-48 modified by the same ligand, but  $\gamma$ -Fe<sub>2</sub>O<sub>3</sub>@MCM-48 still has good capacity for Hg(II) adsorption (1.04 mmol/g) and also has magnetic property. Therefore,  $\gamma$ -Fe<sub>2</sub>O<sub>3</sub>@MCM-48 could be easily separate from the solution after adsorption, compared to the other adsorbents.

#### 4.5 Reusability of the composites

The reusability is an important and desirable property of adsorbent. The reusability of MP-Fe<sub>2</sub>O<sub>3</sub>@MCM-48 was investigated in order to know how many times MP-Fe<sub>2</sub>O<sub>3</sub>@MCM-48 could be reused in Hg(II) adsorption. The experiment was performed by using the same adsorbent in repeated adsorption/regeneration cycles. The initial concentration of Hg(II) solution used in the experiments was 50 mg/L to ensure that MP-Fe<sub>2</sub>O<sub>3</sub>@MCM-48 adsorbent would adsorb Hg(II) at full of its capacity. A solution of 1.0 M thiourea in 2% HCl was used as eluent for adsorbent regeneration. The adsorption time and regeneration time were 1 hour. The results are shown in Figure 4.19.

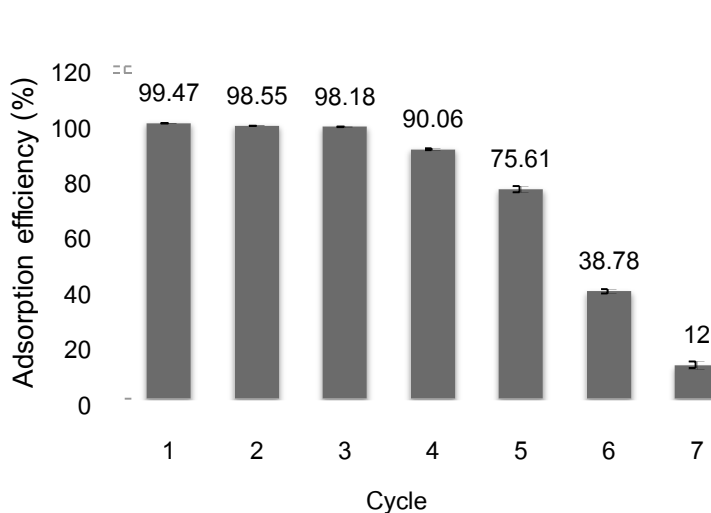


Figure 4.19 Hg(II) adsorption by MP-Fe<sub>2</sub>O<sub>3</sub>@MCM-48 in sequential uses.

In the first, second and third cycles, the adsorbent could adsorb 99.47, 98.55 and 98.18 percent of Hg(II) in solution, respectively. The adsorption efficiency decreased significantly to 90.06% after 3 cycles of use and dramatically decreased after the fifth cycle of use. It is mostly likely because all of Hg(II) ions could not be eluted from active sites when the adsorbents were used in many cycles, resulting in the

decreasing of adsorption efficiency. The results lead to a conclusion that the MP-Fe<sub>2</sub>O<sub>3</sub>@MCM-48 could be used up to 4 cycles before the adsorption efficiency reduced to 75 % and lower.

#### 4.6 Application in real wastewater samples

To demonstrate that MP-Fe<sub>2</sub>O<sub>3</sub>@MCM-48 suits actual use, the adsorbent was applied to remove Hg(II) ions in real wastewater from a refinery plant in Bangkok. The pH of wastewater sample was 1.43 and the concentration of Hg(II) in wastewater sample was determined after digestion of wastewater sample by following the standard method ASTM3223 to convert organic and inorganic mercury compound to mercuric ions. The adsorption experiment was performed in triplicates using 5 mg of MP-Fe<sub>2</sub>O<sub>3</sub>@MCM-48 to extract Hg(II) in 25 mL of wastewater with pH value adjusted to 6 and 60 minutes of adsorption time. The initial concentration of Hg(II) in wastewater was 2.8 and the efficiency in removal of Hg(II) by MP-Fe<sub>2</sub>O<sub>3</sub>@MCM-48 was 99.69 %± 0.1. The results show that MP-Fe<sub>2</sub>O<sub>3</sub>@MCM-48 has good potential as adsorbents for removal of Hg(II) ions in the real wastewater from refinery plant.

## CHAPTER V

### CONCLUSION

A new magnetic composite ( $\gamma\text{-Fe}_2\text{O}_3\text{@MCM-48}$ ) with high surface area and magnetic response was successfully prepared by mixing of MCM-48 and  $\gamma\text{-Fe}_2\text{O}_3$  nanoparticles. The composite was further modified with 3-mercaptopropyl trimethoxysilane (MP- $\text{Fe}_2\text{O}_3\text{@MCM-48}$ ) to improve adsorption affinity toward Hg(II) ions. The adsorbents obtained in each step were characterized by X-ray diffraction spectrometer (XRD), surface area analyzer, Fourier transforms infrared spectrometer (FT-IR), transmission electron microscope (TEM), scanning electron microscope (SEM) and thermogravimetric analysis (TGA). The result from these characterization techniques and the efficiency in Hg(II) adsorption confirmed that MP- $\text{Fe}_2\text{O}_3\text{@MCM-48}$  composite was successfully prepared.

MP- $\text{Fe}_2\text{O}_3\text{@MCM-48}$  composite was applied to remove mercury(II) ion in aqueous solutions using batch method (solid dose of 0.2 g/L) before its determination by cold vapor atomic absorption spectrometer (CVAAS). The effects of pH of Hg(II) solution and extraction time as well as the adsorption isotherms were investigated. The adsorption behavior and suitable conditions of using MP- $\text{Fe}_2\text{O}_3\text{@MCM-48}$  in extraction of Hg(II) ion are summarized in Table 5.1.

**Table 5.1** The adsorption behavior and suitable conditions of the removal of Hg(II) ion

Parameters	Adsorption behavior
Solution pH	6
Time to reach adsorption equilibrium	with in 40 minutes
Adsorption isotherm	Langmuir isotherm
Maximum adsorption capacity (mg/g)	208.3 mg/g

The adsorption of Hg(II) onto MP- $\text{Fe}_2\text{O}_3\text{@MCM-48}$  composite is believed to occur mainly via coordination between Hg ions and -SH groups of MP. MP- $\text{Fe}_2\text{O}_3\text{@MCM-48}$  composite showed much higher efficiency in mercury adsorption, compared to the unfunctionalized  $\gamma\text{-Fe}_2\text{O}_3\text{@MCM-48}$  magnetic composite.

The adsorbents could be regenerated by using acidic thouria solution for elution of adsorbed Hg(II) ions. It was found that MP- $\text{Fe}_2\text{O}_3\text{@MCM-48}$  could be used to

remove Hg(II) ions in solution more than 4 cycles of adsorption/regeneration with high adsorption efficiency. MP-Fe<sub>2</sub>O<sub>3</sub>@MCM-48 was successfully applied to remove Hg(II) ions in the real wastewater from refinery plant. The adsorbents showed a high potential for application in Hg(II) removal from wastewater with a beneficial magnetic property for easy separation.

#### **Suggestion of future work**

- Application to adsorption in large scale including large scale wastewater treatment should be investigated.
- Various eluents and elution condition should be investigated more in detail in order to increase the number of cycle of use.

## REFERENCES

- [1] Tori, N.L. and Mirkin, C.A. Nanostructure in biodiagnostics. Chemical Reviews 105 (2005): 1547-1562.
- [2] Reis, A.T.; Rodrigues, S.M.; Araújo C.; Coelho, J.P.; Pereira, E. and Duarte, A.C. Mercury contamination in the vicinity of a chlor-alkali plant and potential risks to local population. Science of The Total Environment 407 (2009): 2689-2700.
- [3] Liu, M.; Hou, L.; Xi, B.; Zhao, Y. and Xia, X. Synthesis, characterization, and mercury adsorption properties of hybrid mesoporous aluminosilicate sieve prepared with fly ash. Applied Surface Science 273 (2013): 706–716.
- [4] Magos, L. and Clarkson, T.W. The assessment of the contribution of hair to methylmercury extraction. Toxicology Letters 182 (2008): 48-49.
- [5] Namasivayam, C. and Periasamy, K. Bicarbonate-treated peanut hull carbon for mercury (II) removal from aqueous solution. Water Research 27 (1993): 1663-1668.
- [6] Matlock, M.M.; Howerton, B.S. and Atwood, D.A. Chemical precipitation of heavy metals from acid mine drainage Water Research 36 (2002): 4757-4764.
- [7] Oehmen, A.; Viegas, R.; Velizarov, S.; Reis, M. and Crespo, J.G. Removal of heavy metals from drinking water supplies through the ion exchange membrane bioreactor. Desalination 199 (2006): 405-407.
- [8] Siddiqui, W.; Khan, S. and Inamuddin. Synthesis, characterization and ion-exchange properties of a new and novel 'organic–inorganic' hybrid cation-exchanger: Poly(methyl methacrylate) Zr(IV) phosphate. Colloids and Surfaces A: Physicochemical and Engineering Aspects 295 (2007): 193–199.
- [9] Larison, K. and Wiencek, J. Industrial & Engineering Chemistry Research 31 (1992): 2714-2720.



- [10] Aydın, H.; Bulut, Y. and Yerlikaya, C. Removal of copper (II) from aqueous solution by adsorption onto low-cost adsorbents. Journal of Environmental Management 87 (2008): 37–45.
- [11] Quintanilla, D.P.; Hierro, I.D.; Fajardo, M. and Sierra, I. Mesoporous silica functionalized with 2-mercaptopyridine: Synthesis, characterization and employment for Hg(II) adsorption. Microporous and Mesoporous Materials 89 (2006): 58-68.
- [12] Wang, S.G. and Li, J.L. Thiol-functionalized MCM-48: an Effective Absorbent of Mercury Ions. Chinese Chemical Letters 17 (2006): 221-224.
- [13] Schumacher, K.; Grün, M. and Unger, K.K. Novel synthesis of spherical MCM-48. Microporous and Mesoporous Materials 27 (1999): 201-206.
- [14] Rouquevol, J.; Avnir, D.; Fairbridge, C.W.; Evertt, D.; Haynes, J.; Pernicone, N.; Ramsay, J.D.; Sing, K.S.W. and Unger, K.K. Recommendations for the characterization of porous solids. Pure and Applied Chemistry 66 (1994): 1739-1745.
- [15] Beck, J.S. and Vartuli, J.C. Recent advances in the synthesis, characterization and applications of mesoporous molecular sieves. Solid State & Materials Science 1 (1996): 76-87.
- [16] Ursachi, I.; Vasile, A.; Ianculescu, A.; Vasile, E. and Stancu, A. Ultrasonic-assisted synthesis and magnetic studies of iron oxide/MCM-41 nanocomposite. Materials Chemistry and Physics 130 (2011): 1251-1259.
- [17] Wu, X.W.; Ma, H.W.; Li, J.H.; Zhang, J. and Li, Z.H. The synthesis of mesoporous aluminosilicate using microcline for adsorption of mercury(II). Journal of Colloid and Interface Science 315 (2007): 555-561.
- [18] Wu, S.; Li, F.; Xu, R.; Wei, S. and Li, G. Synthesis of thiol-functionalized MCM-41 mesoporous silicas and its application in Cu(II), Pb(II), Ag(I), and Cr(III) removal. Journal of Nanoparticles Research 12 (2010): 2111–2124.
- [19] Fryxell, G.E. The synthesis of functional mesoporous materials. Inorganic Chemistry Communications 9 (2006): 1141-1150.

- [20] Idris, S.A.; Davidson, C.M.; McManamon, C. and Morris, M.A. Large pore diameter MCM-41 and its application for lead removal from aqueous media. Journal of Hazardous Materials 185 (2011): 898-904.
- [21] Hoffmann, F.; Cornelius, M.; Morell, J. and Fröba M. Silica-Based Mesoporous Organic–Inorganic Hybrid Materials. Angewandte Chemie International Edition 45 (2006): 3216-3251.
- [22] Damiá, P.Q.; Isabel, H.; Mariano, F. and Isabel, S. 2-Mercaptothiazoline modified mesoporous silica for mercury removal from aqueous media. Journal of Hazardous Materials B 134 (2006): 245-256.
- [23] Afsaneh, S.; Habibollah, Y. and Alireza, B. Functionalized SBA-15 mesoporous silica by melamine-based dendrimer amines for adsorptive characteristics of Pb(II), Cu(II) and Cd(II) heavy metal ions in batch and fixed bed column Chemical Engineering Journal 168 (2011): 505-518.
- [24] Ritter, H.; Nieminen, M.; Karppinen, M. and Brühwiler, D. A comparative study of the functionalization of mesoporous silica MCM-41 by deposition of 3-aminopropyltrimethoxysilane from toluene and from the vapor phase. Microporous and Mesoporous Materials 121 (2009): 79–83.
- [25] Cui, Z.; Wei, Z. and Shuangxi, L. Synthesis and Characterization of Organofunctionalized MCM-41 by the Original Stepped Templates Sol-Gel Technology. Journal of Physical Chemistry B 109 (2005): 24319-24325.
- [26] Qi, W.; Zuoren, N.; Yali, H.; Zengxiang, C.; Jingxiz, Z. and Wei, W. Direct synthesis of thiol-ligands-functionalized SBA-15: Effect of 3-mercaptopropyltrimethoxysilane concentration on pore structure Material Letter 59 (2005): 3611-3615.
- [27] Elias, V.R.; Oliva, M.I.; Vaschetto, E.G. and Urreta, S.E. Magnetic properties of iron loaded MCM-48 molecular sieves. Journal of Magnetism and Magnetic Materials 322 (2010): 3438-3442.
- [28] Gaslain, F.O.M.; Delacô C.; Walcarius, A. and Lebeau B. One-step preparation of thiol-modified mesoporous silica spheres with various functionalization levels and different pore structure. Journal of Sol-Gel Science and Technology 49 (2009): 112-124.

- [29] Ciesla, U. and Schuth, F. Ordered mesoporous materials. Microporous and Mesoporous Materials 27 (1999): 131-149.
- [30] Tanev, P.T. and Pinnavania, T.J. Mesoporous silica molecular sieves prepared by ionic and neutral surfactant templating: a comparison of physical properties. Chemical of Materials 8 (1996): 2068-2079.
- [31] Zhao, X.S.; Lu, G.Q. and Millar, G.J. Advances in Mesoporous Molecular Sieve MCM-41. Industrial & Engineering Chemistry Research 35 (1996): 2075-2090.
- [32] Raman, N.K.; Anderson, M.T. and Brinker, J. Template-Based Approaches to the Preparation of Amorphous, Nanoporous Silicas Chemical of Materials 8 (1996): 1682-1701.
- [33] Peña, M.L.; Kan, Q.; Corma, A. and Rey, F. Syntnesis of cubic mesoporous MCM-48 materials from the system  $\text{SiO}_2\text{:CTAOH/Br:H}_2\text{O}$ . Microporous and Mesoporous Materials 44-45 (2001): 9-16.
- [34] Voort, P.V.D.; Vercaemst, C.; Schaubroeck, D. and Verpoort, F. Ordered mesoporous materials at the beginning of the third millennium: new strategies to create hybrid and non-siliceous variants. Physical Chemistry Chemical Physics 10 (2008): 347-360.
- [35] Classes of Magnetic Materials [online]. Available from: [http://www.irm.umh.edu/hg2m/hg2m\\_b/hg2m-b.html](http://www.irm.umh.edu/hg2m/hg2m_b/hg2m-b.html). [2009, October 05]
- [36] Ozgur, U.; Alivov, Y. and Morkoc, H. Microwave ferrites, part 1: fundamental properties. Journal of Materials Science: Materials in Electronics 20 (2009): 789–834.
- [37] Chikazumi, S. NewYork., Physics of Magnetism. USA., WILEY & SONS, Inc., 1964.
- [38] Magnetite Mineral Data [online]. Available from: <http://www.webmineral.com/data/Magnetite.shtml>.
- [39] Magnetism and Spintronics [online]. Available from: <http://www.wmi.badw.de/research/spintronics.html> [2012, March 26].
- [40] Cudennec, Y. and Lecerf, A. Topotactic transformations of goethite and lepidocrocite into hematite and maghemite. Solid State Sciences 7 (2005): 520-529.

- [41] Dutta, B.; Jana, S.; Bhattacharjee, A.; Gütlich, P.; Iijima, S.I. and Koner, S.  $\text{Fe}_2\text{O}_3$  nanoparticle in NaY-zeolite matrix: Preparation, characterization, and heterogeneous catalytic epoxidation of olefins. Inorganica Chimica Acta 363 (2010): 696–704.
- [42] Wilhelm, S.M. Mercury in petroleum and gas: Emistification of emission from production, processing, and combustion. United State Environmental Protection Agency: Research and Development. EPA/600/R-01/099 (September 2001).
- [43] Wilhelm, S.M. and Bloom, N. Mercury in petroleum. Fuel pro Technology 63 (2000): 1-27.
- [44] Camel, V. Solid phase extraction of trace element, Spectrochem Acta B 58 (2000): 17-39.
- [45] Bohn, H.L.; Mcneal, B.L. and O'Connor, G.A. Soli Chemistry 3<sup>rd</sup> ed. NewYork., USA., JOHN WILEY & SONS, Inc., 2001.
- [46] Goldberg, S.; Criscenti, L.J.; Tuner, D.R.; Davis, J.A. and Cantrell. K.J. Adsorption-desorption precess in subsurface reactive transport modeling. Vadose Zone Journal 6 (2007): 407-435.
- [47] Antochshuk, J.V.; Jaroniec, M.; Olkhovyk, O.; Park, I.S. and Ryoo, R. Benzoyl thiourea-modified mesoporous silica for mercury(II) removal. Langmuir 19 (2003): 3031-3034.
- [48] Olkhovyk, O.; Antochshuk, V. and Jaroniec, M. Benzoylthiourea-modified MCM-48 mesoporous silica for mercury(II) adsorption from aqueous solutions Colloids and Surfaces A: Physicochemical and Engineering Aspects 236 (2004): 69–72
- [49] Luan, Z.; Fournier, J.A.; Wooten, J.B.; Miser, D.E. and Chang, M.J. Functionalized mesoporous SBA-15 silica molecular sieves with mercaptopropyl group: Preparation, Characterization and application as adsorbent. Surface Science and Catalysis 156 (2005): 897-906.

- [50] Quintanilla, D.P.; Hierro, I.; Fajardo, M. and Sierra, I. Mesoporous silica functionalized with 2-mercaptopyridine: Synthesis, characterization and employment for Hg(II) adsorption. Microporous and Mesoporous Materials 89 (2006): 58–68.
- [51] Quintanilla, D.P.; Hierro, S.; Fajardo, M. and Sierra, I. 2-Mercaptothiazoline modified mesoporous silica for mercury removal from aqueous media Journal of Hazardous Materials B 134 (2006): 245–256.
- [52] Puanggam, M. and Unob, F. Preparation and use of chemically modified MCM-41 and silica gel as selective adsorbents for Hg(II) ions. Journal of Hazardous Materials 154 (2008): 578–587.
- [53] Kolotilova, S.V.; Shvetsa, O.; Cadorb, O.; Kasiana, N.; Pavlov, V.G.; Ouahabb, L.N.; Ilyina, V.G. and Pavlishchuka, V.V. Synthesis, structure and magnetic properties of porous magnetic composite, based on MCM-41 molecular sieve with Fe<sub>3</sub>O<sub>4</sub> nanoparticles Journal of Solid State Chemistry 179 (2006): 2426–2432.
- [54] Emamiana, H.R.; Honarbakhsh-raoufa, A. ; Ataieb, A. and Yourdkhani, A. Synthesis and magnetic characterization of MCM-41/CoFe<sub>2</sub>O<sub>4</sub> nano-composite. Journal of Alloys and Compounds 480 (2009): 681–683.
- [55] Chen, X.; Lam, K.F. and Yeung, K.L. Selective removal of chromium from different aqueous systems using magnetic MCM-41 nanosorbents. Chemical Engineering Journal 172 (2011): 728–734.
- [56] Kima, B.C.; Leeb, J.; Umc, W.; Kimd, J.; Joee, J.; Hyung, J. L.; Kwakc, J.H.; King, J.H.; Leeh, C.; Leeh, H.; Addlemanc, R.S.; Hyeond, T.; Gui, M.B. and Kim, J. Magnetic mesoporous materials for removal of environmental wastes. Journal of Hazardous Materials 192 (2011): 1140–1147.
- [57] Rosenholm, J.M.; Zhang, J.; Sun, W. and Gu, H. Large-pore mesoporous silica-coated magnetite core-shell nanocomposites and their relevance for biomedical applications. Microporous and Mesoporous Materials 145 (2011): 14–20.

- [58] Qiang, Z.; Bao, X. and Ben, W. MCM-48 modified magnetic mesoporous nanocomposite as an attractive adsorbent for the removal of sulfamethazine from water. Water Research (2012): 1e8 chapter3.
- [59] Gies, H.; Grabowski, S.; Bandyopadhyay, M.; Gruenert, W.; Tkachenko, O.B.; Klementiev, K.V. and Birkner, A. Synthesis and characterization of silica MCM-48 as carrier of size-confined nanocrystalline metal oxides particles inside the pore system. Microporous and Mesoporous Materials 60 (2003): 31–42.
- [60] Park, J.; AN, K.; Hwang, Y.; Park, J.G, Noh, H.; Kim, J.Y.; Park, J.H.; Hwang, N.M. and Hyeon, T. Ultra-large-scale syntheses of monodisperse nanocrystals. Nature Materials 3 (2004): 891-895.
- [61] USEPA. B3050, Test Methods for Evaluating Solid Waste. Volume IA: 3rd Edition. EPA/SW-846. National Technical Information Service. Springfield, V. (1986).
- [62] ASTM D3223-95, Standard test method for total mercury in water (Cold-vapor AA). ASTM International. (2007).
- [63] Vero, N.R.; Marcos, I.; Oliv, E.G.; Vaschetto, S.; Urret, G. A.; Eimer, S.P. and Silveti Magnetic properties of iron loaded MCM-48 molecular sieves. Journal of Magnetism and Magnetic Materials 322 (2010): 3438–3442.
- [64] Ciesla, U. and Schuth, F. Ordered mesoporous materials. Microporous and Mesoporous Materials 27 (1999): 131–149.
- [65] Zhang, L.; He, R. and Gu, H.C. Oleic acid coating on the monodisperse magnetite nanoparticles. Applied Surface Science 253 (2006): 2611–2617.
- [66] Girginova, P.I.; Silva, A.L.D.; Lopes, C.B.; Figueira, P. and Otero, M. Silica coated magnetite particles for magnetic removal of  $\text{Hg}^{2+}$  from water. Journal of Colloid and Interface Science 345 (2010): 234–240.
- [67] Fourier transform infrared spectroscopy[Online] West coast analytical service. [online]. Available from: <http://www.wcaslab.com/tech/tbftir.html> [2009, May 18].

- [68] Quintanilla, D.P.; Sánchez, A.; Hierro, I.D.; Fajardo, M. and Sierra, I. Preparation, characterization, and Zn<sup>2+</sup> adsorption behavior of chemically modified MCM-41 with 5-mercapto-1-methyltetrazole. Journal of Colloid and Interface Science 313 (2007): 551–562.
- [69] Li, Y.S.; Wang, Y.; Tran, T. and Perkins, A. Vibrational spectroscopic studies of (3-mercaptopropyl)trimethoxysilane sol–gel and its coating. Spectrochimica Acta Part A 61 (2005): 3032–3037.
- [70] Lia, G.; Zhaob, Z.; Liua, J. and Jiang, G. Effective heavy metal removal from aqueous systems by thiol functionalized magnetic mesoporous silica. Journal of Hazardous Materials 192 (2011): 277–283.
- [71] Kim, C.S.; Rytuba, J.J. and Brown, G.E. EXAFS study of mercury(II) sorption to Fe- and Al-(hydr)oxides: I. Effects of pH. Journal of Colloid and Interface Science 271 (2004): 1-15.

## APPENDIX



The observed amount of  $\gamma\text{-Fe}_2\text{O}_3$  in  $\gamma\text{-Fe}_2\text{O}_3\text{@MCM-48}$  composite in Table 4.1 was calculated according to the following Equations.

$$\text{mmol Fe} = \text{Fe conc.} \frac{\text{mg}}{\text{L}} \times \frac{1\text{L}}{1000 \text{ mL}} \times 100 \text{ mL ext. solution} \times \left( \frac{1 \text{ mmol}}{55.9 \text{ mg Fe}} \right)$$

$$\frac{\text{mmol } \gamma\text{-Fe}_2\text{O}_3}{\text{g composite}} = \text{mmol Fe} \times \frac{1 \text{ mol Fe}_2\text{O}_3}{2 \text{ mol Fe}} \times \frac{1}{10 \text{ mg composite}} \times \frac{1000 \text{ mg composite}}{1 \text{ g composite}}$$

In the synthesis using  $\gamma\text{-Fe}_2\text{O}_3$  at 40-80% of MCM-48 weight, the observed amount of moles of  $\gamma\text{-Fe}_2\text{O}_3$  on the composite were shown in the following table.

**Table A.1** The observed number of moles of  $\gamma\text{-Fe}_2\text{O}_3$  on the composite

Percent $\gamma\text{-Fe}_2\text{O}_3$ added	Fe (mmol)	Observed amount of $\gamma\text{-Fe}_2\text{O}_3$ (mmol/g)
40%	0.0038 $\pm$ 0.0007	0.191 $\pm$ 0.004
50%	0.0051 $\pm$ 0.0009	0.256 $\pm$ 0.005
60%	0.0060 $\pm$ 0.0001	0.301 $\pm$ 0.009
70%	0.0059 $\pm$ 0.0001	0.299 $\pm$ 0.012
80%	0.0060 $\pm$ 0.0006	0.300 $\pm$ 0.003

The theoretical amount of  $\gamma\text{-Fe}_2\text{O}_3$  in the composite is calculated based on 100 % attachment of  $\gamma\text{-Fe}_2\text{O}_3$  on MCM-48 as follows.

In the synthesis using  $\gamma\text{-Fe}_2\text{O}_3$  at 40% of MCM-48 weight, 4 mg of  $\gamma\text{-Fe}_2\text{O}_3$  were mixed with 10 mg of MCM-48. Under ideal condition, 14 mg of composite would be obtained. The number of moles of  $\gamma\text{-Fe}_2\text{O}_3$  (MNPs) on one gram of composite was 1.79 mmol calculated as shown in the following equation

$$\begin{aligned} \frac{\text{mmol MNPs}}{\text{g composite}} &= \frac{4 \text{ mg MNPs}}{14 \text{ mg composite}} \times \frac{1 \text{ mmol MNPs}}{159.72 \text{ mg MNPs}} \times \frac{1000 \text{ mg composite}}{1 \text{ g composite}} \\ &= 1.79 \text{ mmol} \frac{\text{MNPs}}{\text{g composite}} \end{aligned}$$

In the synthesis using  $\gamma\text{-Fe}_2\text{O}_3$  at 40-80% of MCM-48 weight, the theoretical number of moles of  $\gamma\text{-Fe}_2\text{O}_3$  on the composite were shown in the following table.

**Table A.2** The theoretical number of moles of  $\gamma\text{-Fe}_2\text{O}_3$  on the composite

Percent $\gamma\text{-Fe}_2\text{O}_3$ added	Theoretical amount of $\gamma\text{-Fe}_2\text{O}_3$ (mmol/g)
40	1.79
50	2.09
60	2.35
70	2.58
80	2.78

## VITAE

Miss Sumitra Khonsa-nga was born on December 22, 1987 in Kanchanaburi, Thailand. In 2009, she graduated in Bachelor's Degree of Science in Chemistry from Chulalongkorn University. In next year, she began her Master's Degree of Science in program of Petrochemistry and Polymer Science at Chulalongkorn University and completed in 2012.

After that, she had presented "MAGNETIC NANOPARTICLE-MESOPOROUS SILICA MCM-48 COMPOSITES FOR MERCURY(II) ION REMOVAL" in Pure and Applied Chemistry International Conference (PACCON 2013) by poster presentation.

Her present address is 171/28 LPN Pahol-Saphankwai, Pradiphat Road, Samsennai, Phayathai, Bangkok 10400. E-mail address : [flu\\_aor\\_ride@hotmail.com](mailto:flu_aor_ride@hotmail.com)  
Mobile: 089-4859997.